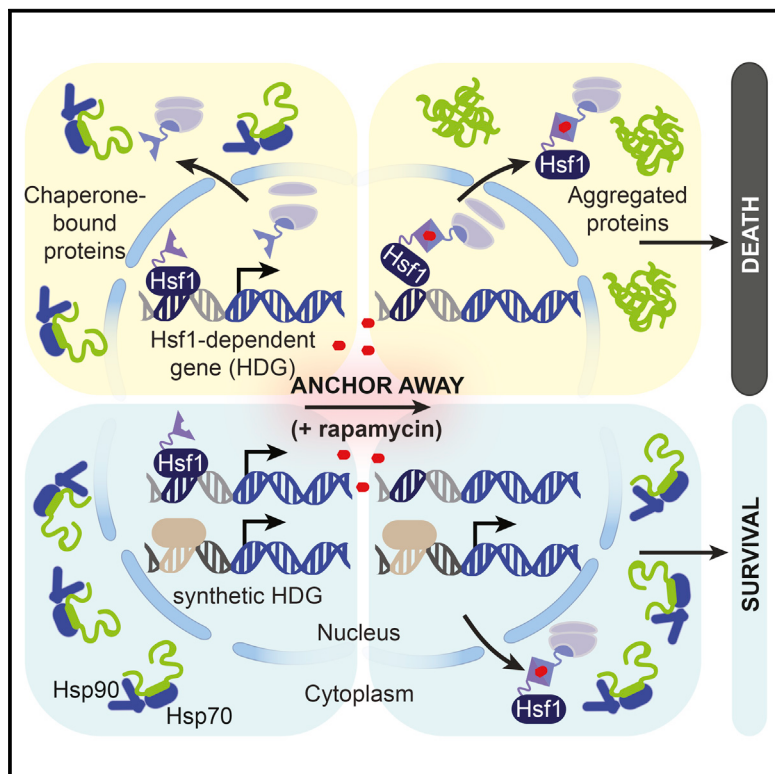


# Molecular Cell

## Defining the Essential Function of Yeast Hsf1 Reveals a Compact Transcriptional Program for Maintaining Eukaryotic Proteostasis

### Graphical Abstract



### Authors

Eric J. Solís, Jai P. Pandey,  
Xu Zheng, ..., Edoardo M. Airoldi,  
David Pincus, Vladimir Denic

### Correspondence

pincus@wi.mit.edu (D.P.),  
vdenic@mcb.harvard.edu (V.D.)

### In Brief

Using a chemical genetics approach for inactivating yeast Hsf1, Solís et al. find that gene expression of a compact chaperone network is minimally sufficient to stave off a lethal proteostasis collapse. Yeast Hsf1 controls both basal and heat stress-induced chaperone expression, whereas mammalian Hsf1 controls only the latter.

### Highlights

- Yeast Hsf1 prevents toxic protein aggregation even in the absence of heat stress
- Basal and heat-induced expression of a small chaperone network is Hsf1 dependent
- Mammalian Hsf1 drives chaperone gene expression during heat stress only
- Rescuing Hsp70 and Hsp90 expression prevents cell toxicity due to Hsf1 ablation

# Defining the Essential Function of Yeast Hsf1 Reveals a Compact Transcriptional Program for Maintaining Eukaryotic Proteostasis

Eric J. Solís,<sup>1,2,8</sup> Jai P. Pandey,<sup>3</sup> Xu Zheng,<sup>3</sup> Dexter X. Jin,<sup>3,4</sup> Piyush B. Gupta,<sup>3,4,5,6</sup> Edoardo M. Airoldi,<sup>7</sup> David Pincus,<sup>3,\*</sup> and Vladimir Denic<sup>1,\*</sup>

<sup>1</sup>Department of Molecular and Cellular Biology, Northwest Labs, Harvard University, Cambridge, MA 02138, USA

<sup>2</sup>Systems Biology PhD Program, Harvard University, Cambridge, MA 02138, USA

<sup>3</sup>Whitehead Institute for Biomedical Research, Cambridge, MA 02142, USA

<sup>4</sup>Department of Biology, Massachusetts Institute of Technology, Cambridge, MA 02139, USA

<sup>5</sup>Koch Institute for Integrative Cancer Research at MIT, Cambridge, MA 02142, USA

<sup>6</sup>Harvard Stem Cell Institute, Cambridge, MA 02138, USA

<sup>7</sup>Department of Statistics, Harvard University, Cambridge, MA 02138, USA

<sup>8</sup>Present address: Yumanity Therapeutics, Cambridge, MA 02139, USA

\*Correspondence: pincus@wi.mit.edu (D.P.), vdenic@mcb.harvard.edu (V.D.)

<http://dx.doi.org/10.1016/j.molcel.2016.05.014>

## SUMMARY

Despite its eponymous association with the heat shock response, yeast heat shock factor 1 (Hsf1) is essential even at low temperatures. Here we show that engineered nuclear export of Hsf1 results in cytotoxicity associated with massive protein aggregation. Genome-wide analysis revealed that Hsf1 nuclear export immediately decreased basal transcription and mRNA expression of 18 genes, which predominately encode chaperones. Strikingly, rescuing basal expression of Hsp70 and Hsp90 chaperones enabled robust cell growth in the complete absence of Hsf1. With the exception of chaperone gene induction, the vast majority of the heat shock response was Hsf1 independent. By comparative analysis of mammalian cell lines, we found that only heat shock-induced but not basal expression of chaperones is dependent on the mammalian Hsf1 homolog (HSF1). Our work reveals that yeast chaperone gene expression is an essential housekeeping mechanism and provides a roadmap for defining the function of HSF1 as a driver of oncogenesis.

## INTRODUCTION

Cells maintain protein homeostasis (proteostasis) in the face of proteotoxic stress, such as heat shock, by inducing expression of genes encoding factors for protein folding and degradation (Hart et al., 2011; Richter et al., 2010). Failure to maintain proteostasis by regulating gene expression has been linked to aging and neurodegeneration (Balch et al., 2008), while many cancers are associated with elevated expression of proteostasis factors (Tang et al., 2015). Yeast heat shock factor 1 (Hsf1) was the first eukaryotic proteostasis transcription factor to be discovered

(Sorger and Pelham, 1987), which enabled the identification of homologous transcription factors across the eukaryotic lineage (Clos et al., 1990; Jakobsen and Pelham, 1991; Rabindran et al., 1991; Scharf et al., 1990). Hsf1 is constitutively nuclear and essential for yeast growth under all conditions (Jakobsen and Pelham, 1988; Sorger and Pelham, 1988). By contrast, mammalian HSF1 is normally dispensable for cell growth absent stress and resides in a repressed state under physiological conditions (Sarge et al., 1993). Following heat shock, however, HSF1 enables thermotolerance by inducing gene expression of proteostasis factors (McMillan et al., 1998; Zhang et al., 2002). Despite these species differences, the core function of mammalian HSF1 is conserved such that a constitutively active version can complement the yeast deletion (Liu et al., 1997). Moreover, as in yeast, HSF1 is constitutively active and essential for proliferation of many cancer cell types (Dai et al., 2007).

Efforts to systematically define genes whose stress-induced expression is dependent on either yeast Hsf1 or mammalian HSF1 have been challenging (Akerfelt et al., 2010). Part of the difficulty comes from gene co-regulation by other transcription factors (Zhang et al., 2002). For example, many heat-activated yeast genes, including several that encode heat shock proteins (HSPs), can be induced by the general stress response factors Msn2 and Msn4 (Boy-Marcotte et al., 1999; Gasch et al., 2000; Treger et al., 1998). There is also the additional challenge in yeast of defining Hsf1's basal transcriptional program, which is presumed to be essential for cell viability because mutations that disrupt either Hsf1 DNA binding or transcriptional activation are lethal (Jakobsen and Pelham, 1991; Torres and Bonner, 1995). Viable partial loss-of-function mutants of Hsf1 that disrupt heat shock-induced gene expression (Eastmond and Nelson, 2006; Morano et al., 1999; Zarzov et al., 1997) cannot resolve whether the basal and heat-induced transcriptional programs are qualitatively distinct or if heat primarily tunes the magnitude of Hsf1's basal transcriptional program. Chromatin immunoprecipitation (ChIP) combined with microarray studies have favored the former possibility by showing that Hsf1 associates with additional promoters under heat stress (Hahn et al., 2004; Lee et al., 2002). By intersecting

these data with heat-induced changes in mRNA abundance detected using DNA microarrays, a list of >160 Hsf1-dependent genes (HDGs) has emerged that is partly devoted to proteostasis and partly to disparate cellular functions such as energy generation, carbon metabolism, and vesicle transport (Eastmond and Nelson, 2006; Hahn et al., 2004).

Hsf1's essential function in the absence of stress is presumably to drive basal gene expression of essential proteostasis factors. However, closer inspection of the Hsf1 target genes challenges this simple conclusion in several ways. First, among Hsf1 gene targets not involved in protein folding, some are individually essential, while pairwise deletions of many non-essential ones result in synthetic lethality (Hahn et al., 2004). Second, it is not known to what extent other basal transcription factors would maintain expression of Hsf1 gene targets involved in protein folding were Hsf1 to be acutely inhibited. Finally, deletion of many non-essential Hsf1 targets results in elevated basal Hsf1 activity (Brandman et al., 2012), suggesting that overexpression of some targets can compensate for the loss of others. One unbiased strategy for defining essential Hsf1 targets would be to systematically place all targets under the control of Hsf1-independent promoters and find which among them are minimally required for life without Hsf1. This synthetic biology approach is conceptually simple, but the lengthiness of the target list renders the prospect of its execution fanciful.

Our starting point was to develop a chemical genetics tool for inducing rapid Hsf1 nuclear export. This enabled us to measure immediate changes in genome-wide basal transcription. From this analysis emerged a list of 18 genes, all but one of which encodes a chaperone, that are strongly dependent on Hsf1 for their basal expression. In addition, we find that Hsf1's repertoire of gene targets is not significantly expanded by heat shock; instead, Hsf1 drives heat-induced chaperone overexpression. With a greatly reduced list of HDGs, we systematically placed all targets under the control of Hsf1-independent promoters to find which among them are minimally required for life without Hsf1. This analysis defined Hsp70 and Hsp90 as the two critical chaperones. Cells engineered to live without Hsf1 were thermosensitive, arguing that survival under severe proteotoxic stress necessitates chaperone overexpression by Hsf1. Last, we used clustered regularly interspaced short palindromic repeats (CRISPR)/Cas9 to create two distinct *hsf1*<sup>-/-</sup> mouse cell lines, which enabled us to define HSF1's core transcriptional program: a set of 9 genes, 8 of which encode chaperones that are functionally akin to HDGs in yeast. However, in mammalian cells, basal chaperone expression is independent of HSF1; rather, HSF1 induced chaperone overexpression following heat shock.

## RESULTS

### A Chemical Genetics Approach Enables Acute Hsf1 Nuclear Depletion at the Physiological Temperature

To develop a tool that acutely inactivates Hsf1 in the absence of stress, we used the “anchor-away” (AA) approach (Haruki et al., 2008). Briefly, we created a yeast strain (Hsf1-AA) that is resistant to Tor1 inhibition by rapamycin and co-expresses an Hsf1-FRB (FKBP rapamycin-binding domain) fusion and a ribosomal protein L13a-FKBP12 fusion (Rpl13A-FKBP12). In this

strain, rapamycin should induce FRB-FKBP12 heterodimerization, thus tethering Hsf1 to nascent ribosome subunits prior to their nuclear export (Figure 1A). Real-time imaging of cells by fluorescence microscopy revealed that rapamycin treatment induced a rapid change in Hsf1-FRB-GFP localization within ~10 min (Figure S1A). Co-expression of a nuclear marker (NLS-mKate2) with Hsf1-FRB-GFP showed that Hsf1-FRB-GFP co-localized with NLS-mKate2 in the nucleus of untreated cells, but after rapamycin treatment, Hsf1-FRB-GFP became cytosolic while NLS-mKate2 remained nuclear (Figures S1B and S1C). ChIP analysis of Hsf1-AA cells demonstrated that rapamycin treatment induced rapid loss of Hsf1 promoter binding for two major chaperone genes (*HSP82* and *SSA1*) (Figure S1D). To functionally test if Hsf1 was removed from chromatin, we used a transcription factor competition assay (Jakobsen and Pelham, 1988) in which GFP is driven by a synthetic promoter with overlapping binding sites for both Hsf1 and a chimeric, β-estradiol-responsive transcription factor (Figures S1E and S1F) (McIsaac et al., 2011). Rapamycin treatment facilitated GFP reporter induction as a function of β-estradiol concentration, suggesting that chromatin-associated Hsf1 was removed as an obstacle to promoter access (Figure S1G). Consistent with this interpretation, rapamycin pretreatment was sufficient to render a distinct GFP reporter of Hsf1-dependent transcription (Brandman et al., 2012) unresponsive to heat shock (Figure S1H). Together, these results demonstrate that Hsf1-AA is a useful tool for acute chromatin and nuclear depletion of Hsf1.

### Hsf1 Prevents Protein Aggregation at the Physiological Temperature

To measure the phenotypic consequences of Hsf1 nuclear export, we incubated Hsf1-AA cells on plates containing rapamycin and observed no colony formation (Figure 1B). This phenotype recapitulates the lethal phenotype of *hsf1*<sup>Δ</sup> cells and was dependent on Hsf1-Rpl13a heterodimerization (Figure S1I), while a second copy of Hsf1 not fused to FRB was able to rescue growth (Figures 1B and S1I). Even though rapamycin treatment of Hsf1-AA cells induced Hsf1 export in a matter of minutes, it took ~2.5 hr before cells became arrested at various stages of the cell cycle (measured by budding index). After extended treatment (>13 hr), some cells lysed asynchronously (Figure S1J), and removal of rapamycin failed to restore cell growth, arguing for irreversible cytotoxicity. Because basal expression of several chaperone genes is dependent on Hsf1 binding sites in their promoters (Erkine et al., 1996; Gross et al., 1993; Nicholls et al., 2009; Sakurai and Ota, 2011), we reasoned that rapid Hsf1 nuclear export is followed by a slower decrease in chaperone concentration, leading to protein aggregation and cytotoxicity. To test this, we measured Hsp70 (Ssa1) and Hsp90 (Hsc82) protein levels following rapamycin treatment by quantitative western blotting. Indeed, 2 hr after Hsf1 inactivation at physiological temperature, Ssa1 and Hsc82 proteins dropped below 30% and 50% of their initial levels, respectively (Figure S1K). Next, we monitored protein aggregation using mCherry fused to a metastable, temperature-sensitive (ts) allele of Ubc9, an established reporter of protein misfolding in yeast that forms cytosolic aggregates visible as fluorescent puncta by microscopy (Kaganovich et al., 2008). In a control experiment, we confirmed that heat shock at 37°C induced

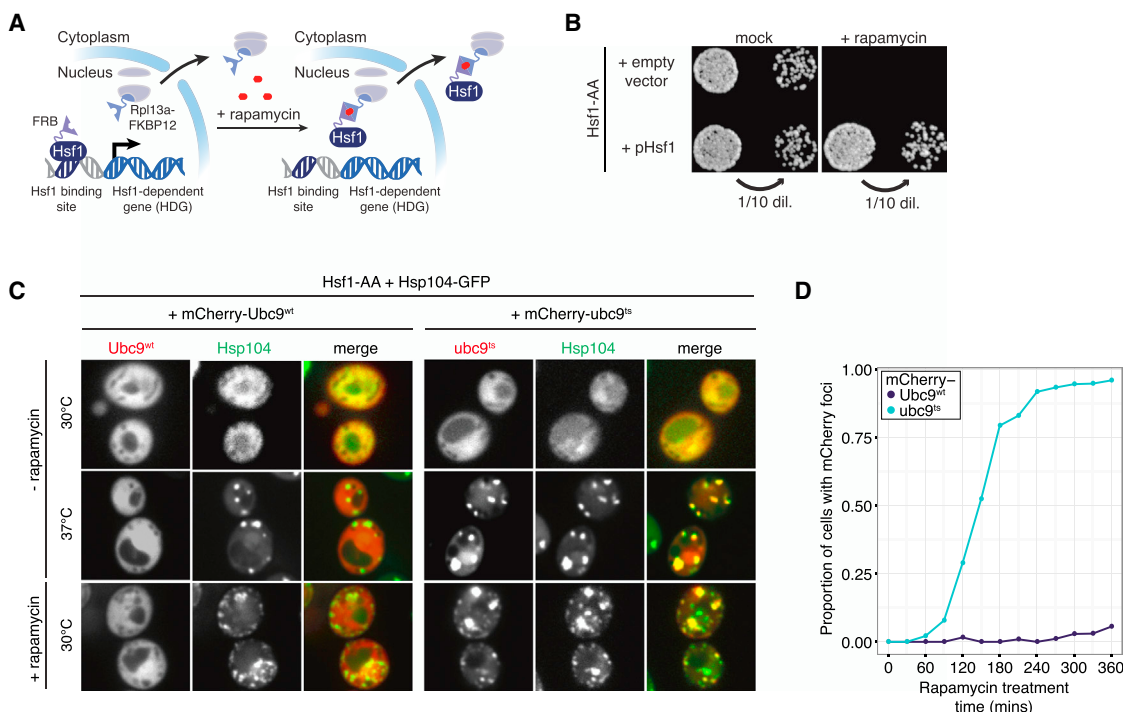


**Figure 1. Acute Inactivation of Hsf1 Induces Proteotoxicity Even in the Absence of Stress**

(A) Schematic of Hsf1-AA.

(B) Hsf1-AA cells with indicated plasmids were spotted at two cell densities onto rapamycin or mock plates. Shown are images of plates incubated for 3 days at 30°C.

(C) Representative confocal micrographs of Hsf1-AA cells expressing endogenous Hsp104-GFP and plasmid-borne mCherry-Ubc9<sup>WT</sup> or -ubc9<sup>ts</sup> taken after logarithmic growth at 30°C, after treatment with heat shock (20 min at 37°C), and after treatment with rapamycin (360 min at 30°C).

(D) Hsf1-AA cells described in (C) were treated with rapamycin for indicated times at 30°C and imaged by epifluorescence microscopy. Blinded images containing at least 100 cells were scored for cells containing mCherry foci and the fraction of scored cells plotted.

See also Figure S1.

mCherry-ubc9<sup>ts</sup>, but not stable mCherry-Ubc9<sup>WT</sup>, to form puncta that co-localized with Hsp104-GFP, a protein disaggregase that localizes to protein aggregates (Glover and Lindquist, 1998) (Figure 1C). Consistent with the timing of the reduction in Hsp70 and Hsp90 levels, we observed mCherry-ubc9<sup>ts</sup> aggregation at the physiological temperature in the majority of cells within 2.5 hr of rapamycin addition (Figure 1D). Importantly, mCherry-Ubc9<sup>WT</sup> remained apparently soluble even after extended rapamycin treatment (Figures 1C and 1D) despite the appearance of Hsp104-GFP puncta in the same cells, which likely mark aggregates of endogenous metastable proteins with similar folding requirements to ubc9<sup>ts</sup> (Figure 1C). Thus, depletion of Hsf1 leads first to decreased expression of chaperones, followed by proteostasis collapse and cell death.

### Yeast Hsf1 Drives Basal Expression of 18 Genes

To define the immediate transcriptional effects of Hsf1 nuclear export, we used native elongating transcript sequencing (NET-seq) (Churchman and Weissman, 2011) to globally track transcription of individual genes in Hsf1-AA cells during a rapamycin treatment time course (15, 30, and 60 min) (Table S1). Statistical analysis (see Experimental Procedures) defined 25 genes that were transcriptionally repressed and 5 that were induced by

15 min of drug treatment ( $p < 10^{-4}$ ) (Figure S2A, left), and these changes persisted at the later time points (Figure S2A, middle and right). To substantiate that the transcriptional changes identified by the NET-seq analysis resulted in bona fide changes in mRNA abundance, we analyzed Hsf1-AA cells treated for 60 min with rapamycin by RNA sequencing (RNA-seq) (Table S2). We observed statistically significant changes in mRNA abundance for 18 of 25 transcriptionally repressed genes and none of the induced genes (Figures 2A, S2B, and S2C; see Experimental Procedures). Importantly, the genes defined by our combined NET-seq/RNA-seq analysis had a strong correlation between the fold decrease in their transcription and their mRNA abundance (Figure S2D).

Given that we defined ~10-fold fewer Hsf1 targets by NET-seq analysis than anticipated (Eastmond and Nelson, 2006; Hahn et al., 2004; Lee et al., 2002), we considered the possibility that technical or biological variability limited our statistical power to detect additional biologically significant transcriptional changes. However, there was no significant difference in the width of confidence intervals, which inversely relate to statistical power, between genes defined by our analysis and other genes (Figure S2E). Another possible source of error was to miss slower transcriptional effects of Hsf1 nuclear export. However, we

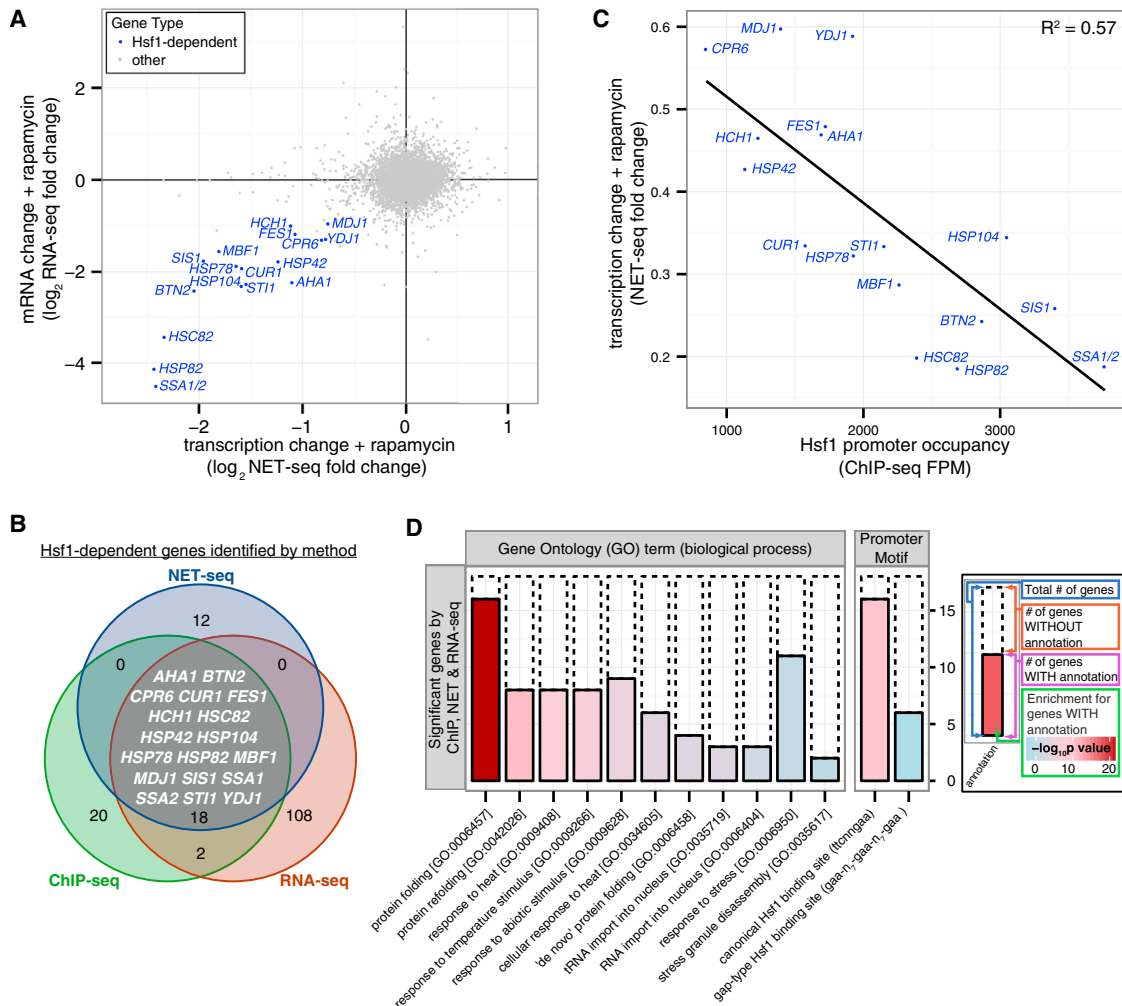


**Figure 2. Hsf1 Drives Basal Expression of a Diverse Set of Protein Folding Factors**

(A) Hsf1-AA cells were grown logarithmically at 30°C and harvested for analysis by NET-seq or RNA-seq immediately prior to and after 15, 30, and 60 min of rapamycin treatment. Shown is a gene scatterplot of transcription versus mRNA changes induced by treatment with rapamycin for 15 and 60 min, respectively.

(B) Venn diagram comparing Hsf1 target genes defined by ChIP-seq, NET-seq, and RNA-seq, with the names of the 18 HDGs detected by all three techniques indicated.

(C) Gene scatterplot of change in HDG transcription resulting from 15 min of rapamycin treatment versus Hsf1 occupancy at HDG promoters.

(D) Bioinformatic analysis of the 18 HDGs defined by ChIP-seq, NET-seq, and RNA-seq. Solid bars show the number of HDGs with the given annotation (Gene Ontology term or promoter motif), and dashed bars show the remaining number of HDGs. The fill color indicates the significance level for the enrichment of the annotated HDGs versus other genes. See Figure S2J for a similar bioinformatic analysis of Hsf1 targets defined by each individual genome-wide approach or by combining any two approaches.

See also Figure S2 and Tables S1, S2, and S3.

defined only three significant changes in transcription after 30 or 60 min of rapamycin treatment (Table S1), and none of these were corroborated by mRNA analysis (Table S2). Rather, transcription of most genes was consistent and largely unperturbed by Hsf1 inactivation, both globally— $R^2 = 0.98$  for all adjacent time points (Figure S2A)—and at the level of individual loci (Figure S2F) across a wide range of expression levels (Figure S2G). Thus, detection of additional Hsf1 targets was not limited by the sensitivity or reproducibility of our analysis.

To independently validate these targets, we monitored Hsf1 DNA binding by ChIP followed by deep sequencing (ChIP-seq).

We isolated chromatin using tandem affinity purification of dual epitope-tagged Hsf1-FLAG-V5 expressed as the only copy of Hsf1 in an otherwise wild-type genetic background. Analysis using a stringent peak-calling algorithm (see **Experimental Procedures**) and bioinformatics identified 40 gene targets (Table S3) with a strong promoter enrichment for Hsf1-binding sites ( $p < 10^{-9}$ ). The ChIP-seq analysis identified none of the 12 NET-seq-only gene targets, while it identified all 18 gene targets corroborated by NET-seq and RNA-seq ( $p < 10^{-42}$ ) (Figures 2B and S2H). Importantly, the genes defined by combined NET-seq/ChIP-seq analysis showed a strong correlation between

fold decrease in transcription and ChIP enrichment (Figures 2C and S2I), arguing that Hsf1 binding to their promoters drives their basal expression.

In summary, we combined three genome-wide approaches (NET-seq, RNA-seq, and ChIP-seq) to define 18 HDGs (Figure 2B), which collectively encode two Hsp70 paralogs (SSA1 and SSA2), both Hsp90 paralogs (HSC82 and HSP82), nucleotide exchange factors and co-chaperones for Hsp70 and Hsp90 (YDJ1, SIS1, FES1, AHA1, HCH1, STI1, and CPR6), nuclear and cytoplasmic aggregases (BTN2, CUR1, and HSP42), mitochondrial protein folding factors (HSP78 and MDJ1), a disaggregase (HSP104), and a cell-cycle transcriptional regulator (MBF1). Bioinformatic analysis of HDG promoters revealed a strong enrichment for consensus Hsf1 binding sites (Sorger and Pelham, 1987) ( $p < 10^{-10}$ ), and gene ontology analysis revealed a strong enrichment for protein folding function ( $p < 10^{-21}$ ) (Figures 2D and S2J). We note that our analysis excludes genes that are regulated by Hsf1 under non-basal conditions, genes that Hsf1 controls redundantly with other transcription factors and genes that use Hsf1 as a pioneer factor (Fujimoto et al., 2012). We conclude that Hsf1 drives a compact transcriptional program in basal conditions.

### The Majority of the Yeast Heat Shock Response Is Hsf1 Independent

We considered the possibility that Hsf1-AA cells attempt to counteract proteotoxicity induced by prolonged rapamycin treatment by secondary changes in gene expression. Indeed, RNA-seq revealed that prolonged rapamycin treatment, which we defined as a comparison between 4 and 1 hr of treatment, caused a >4-fold induction of ~200 genes (Figure S3A), including 4 HDGs (HSP42, HSP72, HSP104, and HSP82). Bioinformatic analysis suggested these changes were associated with alternative metabolism and various stress responses, including heat shock (Figure S3B). To identify the regulators of this response, we analyzed the promoters of induced genes to identify enriched sequence motifs (Carlson et al., 2007), which were cross-referenced with the known sequence specificities of yeast transcription factors (de Boer and Hughes, 2012). This analysis defined a highly enriched ( $p < 10^{-34}$ ), ubiquitous motif that was found in 78% of induced genes, including the 4 strongly upregulated HDGs (Figure S3C). This motif corresponded to the consensus binding site for Msn2 and Msn4 (jointly Msn2/4), two redundant transcription factors activated by a variety of environmental stresses, including heat shock (Causton et al., 2001; Schmitt and McEntee, 1996). Msn2/4 activity is regulated by protein kinase A (PKA), which phosphorylates Msn2/4 under non-stress conditions preventing their nuclear entry (Görner et al., 1998). To test if Msn2/4 activation mimics gene activation induced by prolonged rapamycin treatment, we treated cells expressing analog-sensitive PKA (PKAas) with the ATP-analog 1-NM-PP1, an established chemical genetics approach for inducing Msn2/4 nuclear localization (Hao and O'Shea, 2011). RNA-seq analysis revealed that 1-NM-PP1 treatment of PKAas cells was well correlated with prolonged rapamycin treatment ( $R^2 = 0.70$ ; Figure S3D). Comparative analysis of PKAas *msn2Δ msn4Δ* cells established that Msn2/4 targets ( $p < 10^{-103}$ ) were significantly attenuated (Figures S3E and S3F). These data show that PKA in-

hibition mimics gene expression changes induced by prolonged rapamycin treatment.

Despite its eponymous association with the heat shock response, we observed a remarkable resemblance between the heat shock response and the response to prolonged Hsf1 inactivation (Figure 3A). The similarity between these two responses suggested that gene induction by heat was largely Hsf1 independent and Msn2/4 dependent. To test this, we used NET-seq and RNA-seq to measure the effect of a short rapamycin pretreatment on the heat shock response of Hsf1-AA cells. Consistent with our previous observations, HDGs with multiple Msn2/4 binding sites were still induced by heat shock, while the remaining HDGs were repressed (Figure 3B). Genome wide, the heat shock response remained generally intact in the absence of nuclear Hsf1 ( $R^2 = 0.81$ ), including activation of Msn2/4 targets (Figure 3C). This was supported by Hsf1 ChIP-seq analysis during heat shock, which revealed a list of target genes that significantly overlapped the list of basal targets ( $p < 10^{-59}$ ) (Figure S3G). Unfortunately, our efforts to exploit Hsf1-AA to rigorously define the proximal transcriptional effects of Hsf1 inactivation on the heat shock response were hampered by their convolution with other indirect, secondary changes. When we bioinformatically analyzed gene expression that was significantly reduced by rapamycin pretreatment (Figure S3H), we could not find compelling evidence that Hsf1 directly regulated all but eight of these genes (Figures S3I and S3J and Supplemental Experimental Procedures). Rather, we found that well-established Hsf1-independent components of the heat shock response were exaggerated in its absence (Figures S3H–S3J), which we speculate is due to enhanced heat-induced proteotoxicity absent Hsf1-dependent chaperones (see Supplemental Experimental Procedures).

As an alternative to heat stress, we took advantage of the known observation that heat shock and PKA inhibition have similar effects on cell growth, protein synthesis, and the activity of multiple transcription factors, including Msn2/4 (Causton et al., 2001; Smith et al., 1998; Thevelein and de Winde, 1999). Indeed, 1-NM-PP1 treatment of PKAas Hsf1-AA cells induced a change in the transcriptome that resembled the heat-shock response ( $R^2 = 0.76$ ) (Figure 3D), as well as prolonged rapamycin treatment (Figure S3D). Yet, unlike these responses, PKA inhibition did not trigger mCherry-ubc9<sup>ts</sup> aggregation (Figure S3K), affording us the opportunity to probe Hsf1's role in co-activating the bulk of the heat shock response. Strikingly, rapamycin pretreatment of PKAas Hsf1-AA cells had a minor effect on genome-wide expression changes induced by 1-NM-PP1 treatment ( $R^2 = 0.95$ ) (Figure 3E), including the induction of Msn2/4 targets (Figure S3L). Rapamycin only led to the reduced expression of HDGs without multiple Msn2/4 binding sites in their promoters (Figure 3F). These data support the notion that Msn2/4 drive expression of the majority of heat shock-induced genes independent of Hsf1.

### Mammalian HSF1 Drives a Core Transcriptional Program of Nine Genes during Heat Shock

Mammalian cells have multiple heat shock factors (e.g., HSF1, 2, 4, 5, X, and Y in the human genome), homologous to yeast Hsf1 (Akerfelt et al., 2010). None are normally essential for viability in

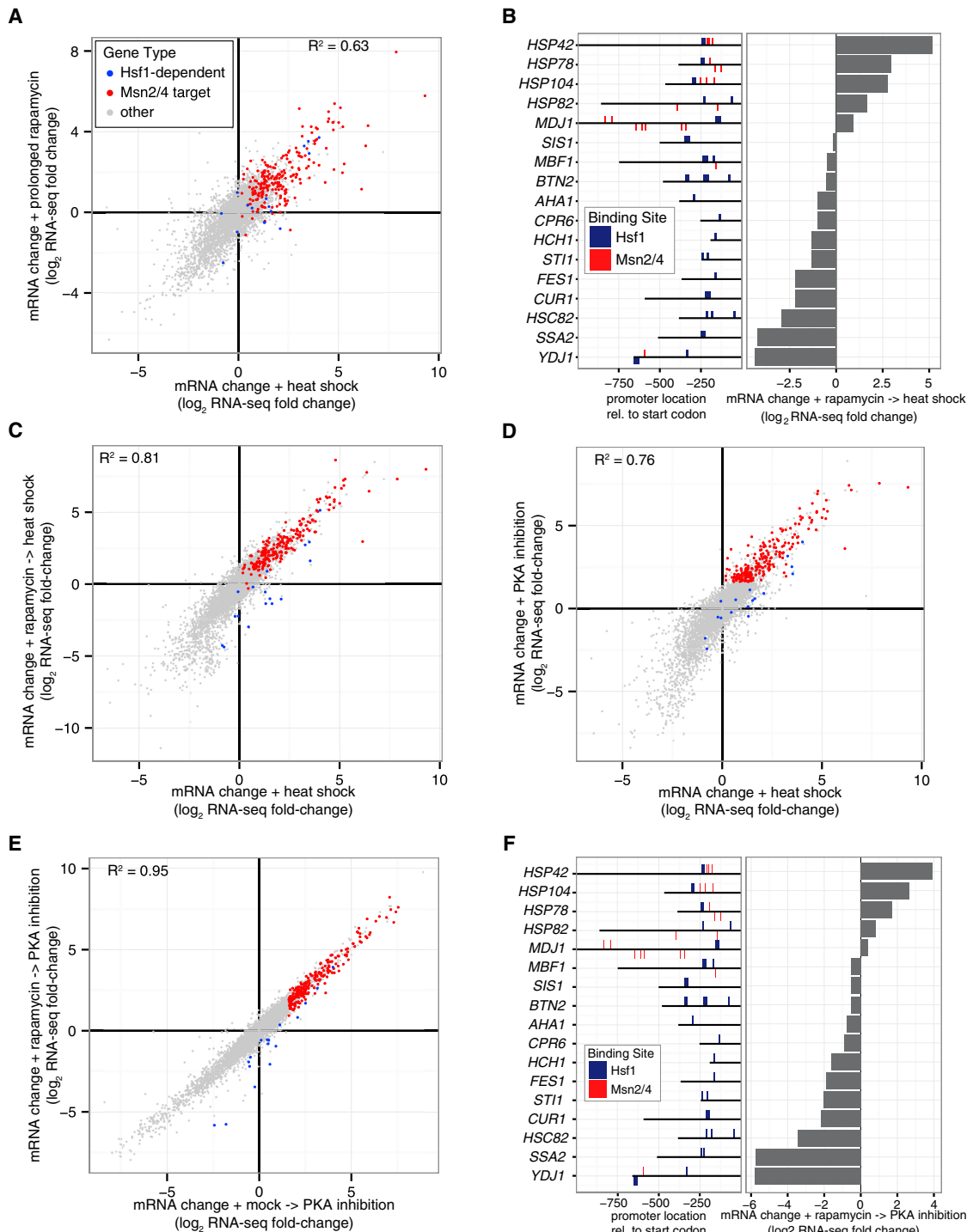


**Figure 3. Induction of Most Genes by Heat Shock Is Hsf1 Independent and Msn2/4 Dependent**

(A) Hsf1-AA cells were grown at 30°C and heat shocked (39°C for 30 min) or treated with rapamycin for either 60 or 240 min at 30°C prior to harvesting for analysis by RNA-seq. Shown is a gene scatterplot of mRNA changes induced by prolonged rapamycin treatment (240 versus 60 min) (y axis) versus changes induced by heat shock (x axis). Msn2/4 targets were defined as genes with at least one Msn2/4 promoter binding site (AGGGG) that were in the top 10% of genes induced by PKA inhibition (see Figure 3D).

(B) Left: locations of predicted bindings sites for Hsf1 (TTCnnGAA and TTC-n<sub>7</sub>-TTC-n<sub>7</sub>-TTC) and Msn2/4 (AGGGG) in HDG promoters. Right: Hsf1-AA cells were grown logarithmically at 30°C (control) or treated with rapamycin (30°C for 30 min) followed by heat shock (39°C for 30 min) prior to harvesting for RNA-seq analysis. Shown are HDG mRNA changes induced by sequential treatment relative to control.

(legend continued on next page)

the absence of stress, but loss of HSF1 uniquely renders cells heat sensitive and unable to acquire thermotolerance (McMillan et al., 1998; Zhang et al., 2002). Comparison of heat-induced changes in mRNA abundance measured by DNA microarray analysis in wild-type mouse embryonic fibroblasts (MEFs) versus those derived from a *hsf1*<sup>-/-</sup> mouse has led to a long list of HDGs (Trinklein et al., 2004). To define what fraction of these changes represent the core HSF1 transcriptional program that is shared across many cell types and differentiation states, we used CRISPR/Cas9-mediated genome editing to generate *hsf1*<sup>-/-</sup> mouse embryonic stem cells (mESCs) and *hsf1*<sup>-/-</sup> MEFs (Figures S4A and S4B). Next, we measured mRNA abundance by RNA-seq in *hsf1*<sup>-/-</sup> mESCs and MEFs in reference to their wild-type counterparts both in unstressed cells and following heat shock (Table S4). In unstressed cells, the transcriptomes of the wild-type and *hsf1*<sup>-/-</sup> cells were remarkably similar (Figure S4C). Only two genes were significantly upregulated and two genes were significantly downregulated in both cell types ( $p = 0.33$  for both) (see Experimental Procedures), approximately the number of significant observations one would expect by random chance. There was no functional enrichment among these genes, and none encode chaperones. We conclude that HSF1 has little or no effect on basal transcription that is common to both mESCs and MEFs.

To define HSF1's core transcriptional program during heat shock, we first asked which genes are heat induced in both wild-type mESCs and MEFs and found 20 genes ( $p < 10^{-18}$ ), many of which encode chaperones (Figure 4A). Next we asked which genes showed reduced expression in *hsf1*<sup>-/-</sup> cells compared to wild-type cells following heat shock in both mESCs and MEFs and found 15 genes ( $p < 10^{-11}$ ), again including many chaperone genes (Figure 4B). By intersecting these two gene lists, we found only 9 genes that were induced by heat shock in both wild-type mESCs and MEFs and repressed in both heat-shocked *hsf1*<sup>-/-</sup> cell types (Figure 4C). We define these 9 genes as the core mammalian HDGs and note that 8 of 9 form a densely linked interaction network with the cytosolic Hsp40, Hsp70, and Hsp90 chaperones at its center (Figure 4D). The structure of this network is remarkably similar to the one formed by yeast HDGs (Figure 4E).

Hsf1 is the sole factor in yeast that controls both basal and heat-induced expression of HDGs. By contrast, mammalian HSF1 is dispensable for high basal expression of HDGs. We wondered if HSF2, the only other HSF paralog with detectable expression in both the mESCs and the MEFs, was responsible. Thus, we generated *hsf2*<sup>-/-</sup> MEFs and *hsf1*<sup>-/-</sup> *hsf2*<sup>-/-</sup> double-mutant MEFs and measured mRNA abundance by RNA-seq in

unstressed cells in comparison wild-type and *hsf1*<sup>-/-</sup> MEFs. In the absence of HSF2, mRNA levels for three HDGs—two Hsp70 homologs (HSPA1A and HSPA1B) and one Hsp90 homolog (HSP90AB1)—were significantly upregulated ( $p < 10^{-4}$ ) (Figure S4D), but we found that the basal expression of all HDGs in *hsf1*<sup>-/-</sup> *hsf2*<sup>-/-</sup> MEFs was similar to wild-type (Figures 4F and S4E). Taken together, these data strongly argue that the HSF family does not control basal expression of chaperones in MEFs.

### A Synthetic Transcriptional Program Bypasses Hsf1's Essential Function

In mammalian cells, high HSF1-independent basal expression of chaperone genes may explain why HSF1 is not essential in the absence of stress. This prompted us to ask if the essential function of yeast Hsf1 can be obviated by constitutive expression of HDGs from Hsf1-independent promoters. To this end, we constructed four plasmids carrying in total 15 HDG open reading frames—we excluded SSA1, HSP82, and HCH1 because they are redundant with their paralogs (SSA2, HSC82, and AHA1, respectively)—under the control of promoters from highly expressed housekeeping genes (Figures 5A and S5A). We termed these “synthetic HDGs” (synHDGs). Consistent with the idea that HDG expression provides negative Hsf1 feedback to maintain proteostasis, we found that Hsf1-AA cells expressing synHDGs had reduced Hsf1 basal activity (Figure S5B). Strikingly, even in the presence of rapamycin these cells continued to robustly proliferate (Figure 5B) and no longer formed visible mCherry-ubc9<sup>ts</sup> aggregates (Figures 5C and S5C). To test if constitutive expression of chaperones can enable cells to live in the complete absence of Hsf1, we introduced synHDG expression plasmids into *hsf1*<sup>-/-</sup> cells carrying an Hsf1 expression plasmid. Following plasmid shuffling, we found that *hsf1*<sup>-/-</sup> cells expressing synHDGs grew comparably to cells with a second Hsf1 expression plasmid (Figure S5D). Further, RNA-seq analysis did not reveal any coherent secondary changes to gene expression between these strains (Figure S5E).

### The Essential Function of Hsf1 Is to Drive High Basal Co-expression of Hsp70 and Hsp90

To determine if all 15 synHDGs were necessary to bypass the essential function of Hsf1, we transformed Hsf1-AA cells with subsets of the four expression plasmids and found that only two were necessary (Figure S5F): the plasmid containing SSA2 (Hsp70), along with three other synHDGs, and the plasmid containing HSC82 (Hsp90) and two other synHDGs. By deleting individual synHDGs on these two plasmids, we found that that only SSA2 and HSC82 were indispensable for Hsf1 bypass

(C) Hsf1-AA cells were grown at 30°C (control) or treated with either rapamycin (30 min at 30°C) and then heat shock (39°C for 30 min) or carrier only and then heat shock prior to harvesting for RNA-seq analysis. Shown is a gene scatterplot of mRNA changes induced by the two treatments relative to the control.

(D) Hsf1-AA PKAas cells were grown at 30°C (control) or treated with heat shock (39°C for 30 min) or the PKA inhibitor 1-NM-PP1 (30°C for 30 min) prior to harvesting for RNA-seq analysis. Shown is a gene scatterplot comparing mRNA changes induced by these two treatments relative to control.

(E) Hsf1-AA PKAas cells were grown at 30°C or after treatment with either rapamycin (30 min at 30°C) and then 1-NM-PP1 (30 min at 30°C) or carrier-only and then 1-NM-PP1 prior to harvesting for RNA-seq analysis. Shown is a gene scatterplot comparing mRNA changes induced by these two treatments relative to control.

(F) Left: HDG promoter locations of Hsf1 and Msn2/4 binding sites as in (B). Right: Hsf1-AA PKAas cells were grown at 30°C (control) or after treatment with rapamycin (30 min at 30°C) and then 1-NM-PP1 (30 min at 30°C) prior to harvesting for RNA-seq analysis. Shown are HDG mRNA changes induced by sequential treatment relative to control.

See also Figure S3.

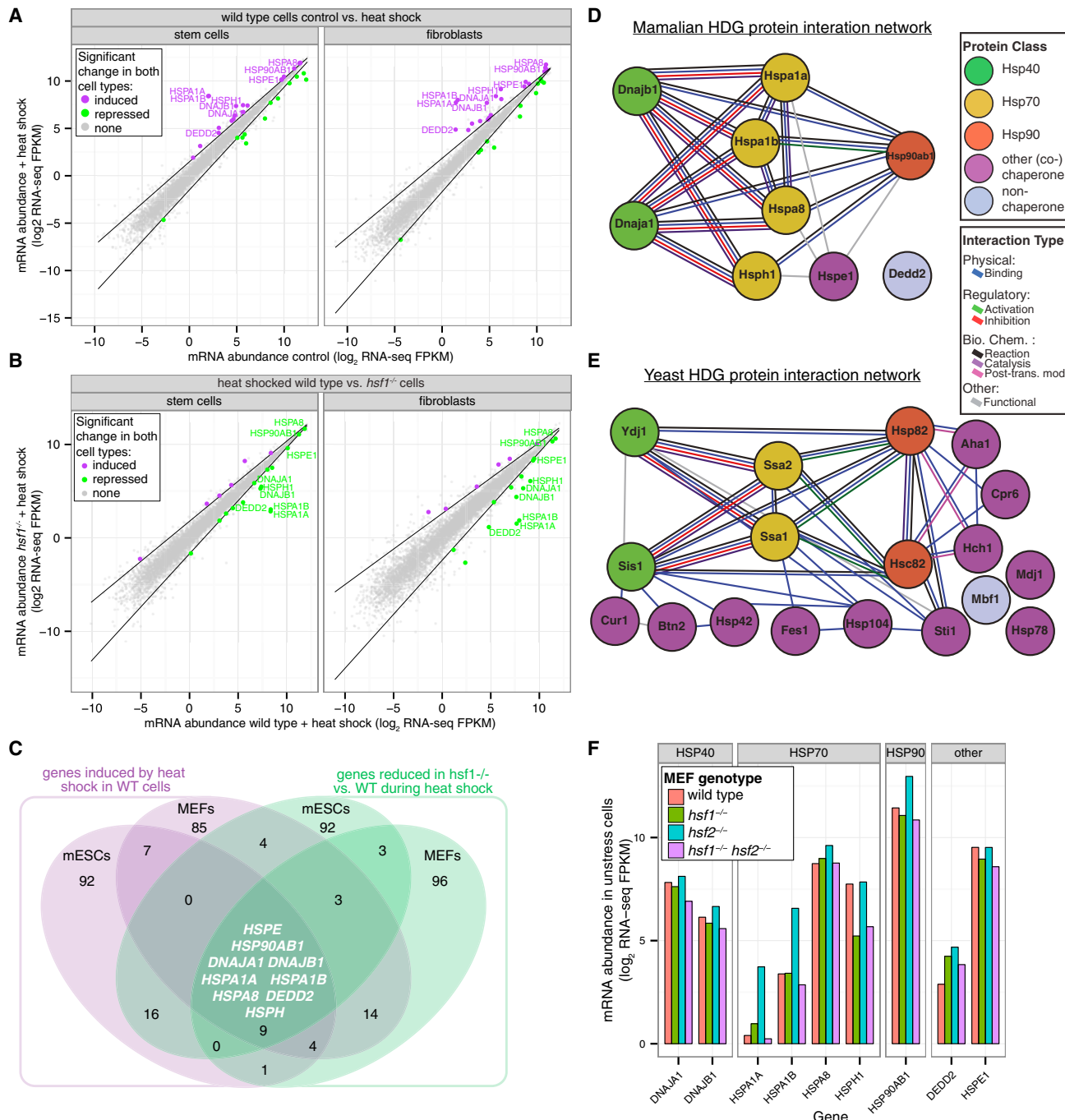


**Figure 4. Mammalian HSF1 Enables Heat Induction of a Chaperone Network Similar to the Yeast HDG Network**

(A) Wild-type mESCs and MEFs were cultured at 37°C or treated with heat shock (42°C for 60 min) prior to harvesting for RNA-seq analysis. Shown is a gene scatterplot of mRNA abundances in treated versus control samples for each cell type. Dark lines indicate statistical thresholds used to define genes with significant changes in expression (see Experimental Procedures), and genes with significant changes in both cell types are colored. Also indicated are gene names of HDGs defined by additional experiments and analyses (see Figures 4B and 4C and Experimental Procedures).

(B) Wild-type (WT) and *hsf1*<sup>-/-</sup> mESCs and MEFs were heat shocked (42°C for 60 min) and then analyzed by RNA-seq. Shown is a gene scatterplot of mRNA abundances in heat shocked WT versus *hsf1*<sup>-/-</sup> cells for each cell type. For definition of dark lines and gene names, see (A).

(C) Venn diagram comparing genes in mESCs and MEFs that are significantly induced by heat shock in WT cells (purple) with genes whose expression is significantly reduced during heat shock in *hsf1*<sup>-/-</sup> versus WT cells. HDGs are defined as genes in the four-way intersection and their names indicated.

(legend continued on next page)

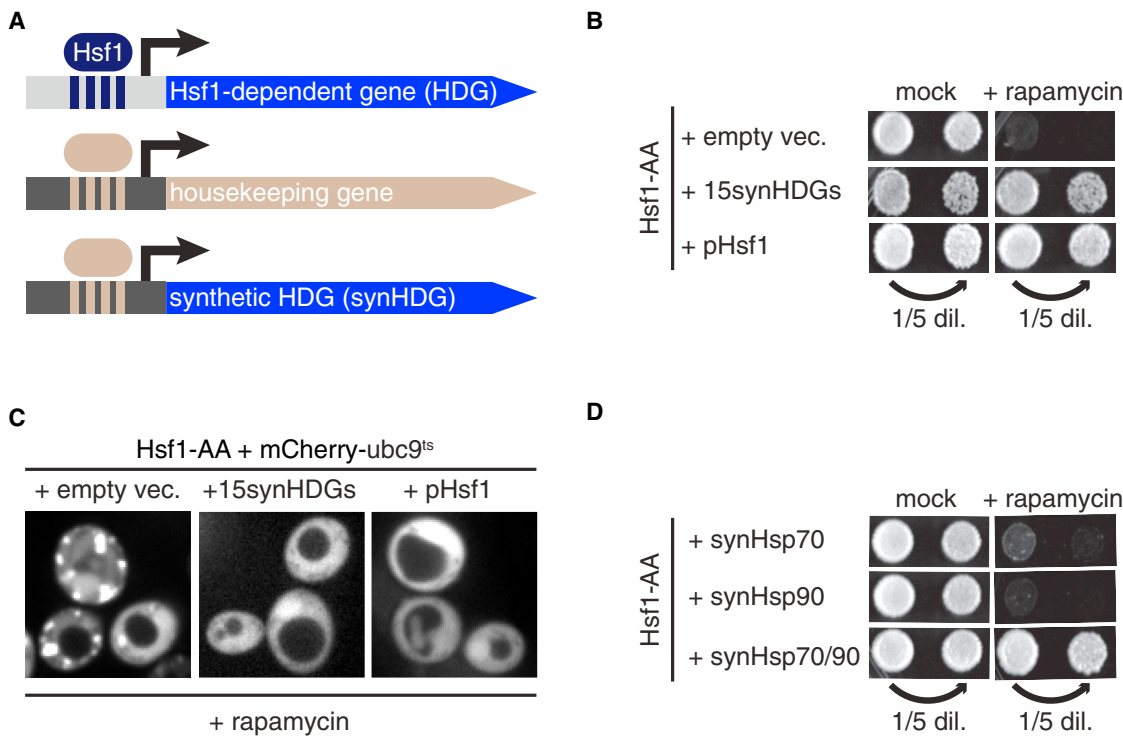


**Figure 5. A Synthetic Transcriptional Program Reveals the Essential Function of Hsf1**

(A) Schematic of promoter swapping strategy for constitutive expression of Hsf1 targets from strong Hsf1-independent promoters. See Figure S5A for details. (B) Hsf1-AA cells with indicated plasmids were spotted at two concentrations onto rapamycin or mock (carrier-only) plates. Shown are images of plates incubated for 5 days at 30°C.

(C) Representative confocal micrographs of Hsf1-AA cells expressing plasmid-borne mCherry-ubc9<sup>ts</sup> and indicated plasmids taken after treatment with rapamycin (360 min at 30°C).

(D) Hsf-AA cells with indicated transgenes were spotted at two concentrations onto rapamycin or mock plates, which also contained β-estradiol to drive synHsp expression from β-estradiol-dependent promoters (see Experimental Procedures for details). Shown are images of plates incubated for 5 days at 30°C. See also Figure S5 and Table S5.

(Figure S5G). Impressively, co-expression of just SSA2 and HSC82, but neither gene expressed alone, enabled Hsf1-AA cells to robustly grow without apparent mCherry-ubc9<sup>ts</sup> aggregation in the presence of rapamycin (Figures 5D and S5H). These data demonstrate that the minimal essential function of Hsf1 is to drive high basal gene expression of Hsp70 and Hsp90. Although it may not be surprising that cells require high levels of Hsp70 and Hsp90 to live, it is remarkable that Hsf1's required contribution to cell viability can be pared down to the expression of only two chaperone genes.

Hsf1 activity is adjusted to the state of protein folding in the cell (Anckar and Sistonen, 2011; Wu, 1995). By contrast, Hsf1-AA cells expressing synHDGs lack this transcriptional feedback and should be susceptible to proteotoxic stress in the presence of rapamycin. Consistent with this notion, we found that Hsf1-AA cells expressing the synHDGs showed marked growth impairment on rapamycin plates at the elevated

temperature of 37°C (Figure S5I). As an attempt to improve growth at 37°C, we introduced additional copies of synSSA2 and synHSC82 but observed only a modest improvement (Figure S5I). These data argue that coordinated homeostatic control of HDG expression by Hsf1 is required for fitness at elevated temperature.

## DISCUSSION

Heat shock factors make up one of the most conserved families of sequence-specific transcription factors (Wu, 1995). In all eukaryotes that have been examined, they have been implicated in the induction of HSP genes as a response to proteotoxic stress. However, mechanistic dissection of this deeply conserved core function has been challenging because members of this family have been deployed differentially through evolution to perform specific functions. In particular, yeast Hsf1 performs

(D and E) Mammalian and yeast HDG protein-protein interaction network (see Experimental Procedures).

(F) Wild-type, *hsf1*<sup>-/-</sup>, *hsf2*<sup>-/-</sup>, and *hsf1*<sup>-/-</sup> *hsf2*<sup>-/-</sup> MEFs were cultured at 37°C prior to harvesting for RNA-seq analysis. Shown are mRNA abundances for HDGs in each cell line.

See also Figure S4 and Table S4.

an essential function in all conditions, whereas mammalian HSF1 is dispensable for normal cell growth but becomes essential during oncogenic transformation (Dai et al., 2007). Here we used comparative genomics to understand how yeast Hsf1 and mammalian HSF1 have diverged from each other.

Lack of a suitable tool for acutely inactivating yeast Hsf1 has been a major obstacle to defining its function. Here we used “anchor away” to induce rapid Hsf1 nuclear export following rapamycin addition (Hsf1 AA) and studied the immediate and long-term transcriptional consequences at the physiological temperature. By combining information from three independent genome-wide approaches (NET-seq, RNA-seq, and ChIP-seq), we were able to define an unexpectedly small number of HDGs. We found that corroboration of putative target genes by independent genomic approaches yielded a great increase in specificity and reproducibility, without any apparent decrease in sensitivity, even when the number of targets defined by each approach differed significantly (Figure S2J). Our study should serve as a roadmap for revisiting other transcription factor target lists, as well as defining the gene targets of poorly characterized transcription factors.

We also found that prolonged Hsf1 AA triggered a global change in gene expression resembling the heat shock response. Controlled heat shock experiments and a chemical genetics approach that mimics heat as a stimulus revealed that the heat shock response remains largely intact upon Hsf1 AA. Thus, the majority of the yeast heat shock response is the job of distinct general stress responsive transcription factors. Retrospectively, our study illustrates how earlier genomic approaches to dissect out Hsf1 gene targets from the complexities of the heat shock response have obscured the simplicity of Hsf1’s role in maintaining proteostasis: Hsf1 tunes expression of a compact regulon according to the protein folding needs of the cell. Our work also provides a complementary perspective to an earlier yeast proteomic analysis of proteins induced by cytosolic expression of a misfolded mutant protein, which post hoc analysis revealed are strongly enriched for HDGs (12 of 27 are HDGs;  $p < 10^{-21}$ ) (Geiler-Samerotte et al., 2011). Although Hsf1’s contribution to proteotoxic stress is limited, it is critical, as cells we engineered to bypass Hsf1’s essential function with constitutive basal expression of synHDGs have diminished fitness at elevated temperature. This now provides a starting platform for introducing negative transcriptional feedback control of synHDGs to enable full functional replacement of Hsf1 with a synthetic proteostasis circuit.

Yeast Hsf1 is part of an essential transcriptional feedback loop that operates even at the physiological temperature. By contrast, we found that the mammalian HSF family is dispensable for cell growth in the absence of stress in two independent mouse cell types. The HSF1 core transcriptional program comprised nine genes and was revealed only following heat shock. A complementary recent study has ascribed a similarly restricted role for HSF1 in the mammalian heat shock response (Mahat et al., 2016). Remarkably, eight of nine genes encoded chaperones that are organized into a strikingly similar functional network as the yeast HDGs (Figures 4D and 4E). This provides a satisfying denouement for the previous seminal discovery that a constitutively active mutant of human HSF1 enables yeast cells to live

without Hsf1 (Liu et al., 1997). We speculate that HSF1 is dispensable in unstressed mammalian cells because a distinct transcription factor or factors maintain high basal expression of HSPs. Although we do not have any experimental evidence for the identity of this factor or factors, preliminary analysis of the promoters of the mammalian HDGs revealed enrichment for the E-box motif that is bound by the Myc/Max heterodimer (Desbarats et al., 1996). Myc is a potent, pro-growth transcriptional activator of ribosome biogenesis and many cancers depend on Myc oncogenic activity. Perhaps Myc enables coordination between chaperone protein gene expression and transcriptional control of ribosome biogenesis to provide sufficient chaperones for newly synthesized proteins. This raises the interesting possibility that multi-cellular organisms evolved a larger chaperone buffer under basal conditions by uncoupling expression of HSPs from HSF1 while still maintaining HSP expression control by HSF1 under extreme conditions. Malignant growth is a case in point because in this context HSF1 inhibition results in cell proliferation arrest (Dai et al., 2007) and the accumulation of toxic protein aggregates (Tang et al., 2015). Surprisingly, HSF1 appears to drive a transcriptional program distinct from heat shock in cancer cells (Mendillo et al., 2012). Establishing the oncogenic contribution of HSF1 core gene targets defined by our work versus the cancer-specific gene targets is an important future goal. By demonstrating the superior contribution of Hsp70 and Hsp90 to Hsf1-mediated proteostasis in yeast, our work also provides the impetus for testing whether Hsp70 and Hsp90 inhibitors have synergistic anti-neoplastic effects on HSF1-dependent cancers.

## EXPERIMENTAL PROCEDURES

### Yeast Strains and Plasmids

Yeast strains used in this work are detailed in Table S5, and plasmids used as well as growth conditions are described in detail (see *Supplemental Experimental Procedures*).

### Anchor-Away Experiments

Unless otherwise indicated, 1 μM rapamycin was used to anchor away Hsf1-FRB in a rapamycin-resistant background (*TOR1-1 fpr1Δ*) (see *Supplemental Experimental Procedures* for detailed experimental conditions for microscopy, flow cytometry, and western blotting).

### NET-Seq, RNA-Seq, and ChIP-Seq Experiments

Genome-wide next-generation sequencing experiments and analysis are described in detail along with statistical and bioinformatics methods (see *Supplemental Experimental Procedures*).

### Mammalian Cell Lines and Genetic Manipulation

Wild-type MEFs and mESCs were obtained from Jackson Laboratories (Immortalized MEFs: CBA316; mESCs: 129X1/SvJ strain). CRISPR/Cas9 procedures and validation are described in detail along with immunofluorescence and western blotting procedures (see *Supplemental Experimental Procedures*).

## SUPPLEMENTAL INFORMATION

Supplemental Information includes Supplemental Discussion, Supplemental Experimental Procedures, five figures, and six tables and can be found with this article online at <http://dx.doi.org/10.1016/j.molcel.2016.05.014>.

**AUTHOR CONTRIBUTIONS**

V.D., D.P., and E.J.S. conceived of the project and designed the experiments. E.J.S. performed the cloning and yeast strain construction. E.J.S. developed the quantitative microscopy, flow cytometry, and genetics assays and performed these experiments with the Hsf1-AA strain, with help from D.P. for live-cell confocal microscopy. V.D. performed the NET-seq experiments. X.Z. performed the ChIP-seq experiments. E.J.S. and D.P. prepared yeast samples, from which D.P. purified RNA, for RNA-seq. J.P.P., D.X.J., and P.B.G. developed the CRISPR/Cas9 genome editing protocol. J.P.P. and D.X.J. generated the Hsf1 knockout cell lines. J.P.P. prepared mammalian cell samples for RNA-seq. E.J.S., D.P., and V.D. analyzed the data with help from E.M.A. E.J.S., D.P., and V.D. made the figures and wrote the paper. All authors edited the manuscript.

**ACKNOWLEDGMENTS**

We thank S. Churchman and B. Tye for reagents and assistance with NET-seq experiments and data analysis; J. Krakowiak for technical assistance with RNA preps; A.S. Hansen for *TPKas* strains and 1-NM-PP1; W. Reilly for generating HDG knockout plasmids; J. Offermann for reagents; P. Arvidson for administrative support; P. Stoddard, Q. Justman, B. Zid, and R. Subramanian for useful discussions; P. Rogers for flow cytometry and general support; members of the V.D. and Lindquist labs for comments and suggestions; C. Chan for help with figures; and S. Churchman, A. Murray, J. Taunton, L. Whitesell, B. Stern, J. Stewart-Ornstein, B. Tye, C. Chan, and C. Shoemaker for helpful comments on the manuscript. This work was supported by the National Institute on Aging R21 grant (R21 AG050134-01 to V.D.) and Kirschstein National Research Service Award diversity fellowship (F31 AG044967-03 to E.S.), a National Institutes of Health Early Independence Award (DP5 OD017941-01 to D.P.), and a Cancer Research Fellowship from the Alexander and Margaret Stewart Trust (D.P.).

Received: January 21, 2016

Revised: March 22, 2016

Accepted: May 11, 2016

Published: June 16, 2016

**REFERENCES**

- Akerfelt, M., Morimoto, R.I., and Sistonen, L. (2010). Heat shock factors: integrators of cell stress, development and lifespan. *Nat. Rev. Mol. Cell Biol.* **11**, 545–555.
- Ankar, J., and Sistonen, L. (2011). Regulation of HSF1 function in the heat stress response: implications in aging and disease. *Annu. Rev. Biochem.* **80**, 1089–1115.
- Balch, W.E., Morimoto, R.I., Dillin, A., and Kelly, J.W. (2008). Adapting proteostasis for disease intervention. *Science* **319**, 916–919.
- Boy-Marcotte, E., Lagniel, G., Perrot, M., Bussereau, F., Boudsocq, A., Jacquet, M., and Labarre, J. (1999). The heat shock response in yeast: differential regulations and contributions of the Msn2p/Msn4p and Hsf1p regulons. *Mol. Microbiol.* **33**, 274–283.
- Brandman, O., Stewart-Ornstein, J., Wong, D., Larson, A., Williams, C.C., Li, G.-W., Zhou, S., King, D., Shen, P.S., Weibezahn, J., et al. (2012). A ribosome-bound quality control complex triggers degradation of nascent peptides and signals translation stress. *Cell* **151**, 1042–1054.
- Carlson, J.M., Chakravarty, A., DeZiel, C.E., and Gross, R.H. (2007). SCOPE: a web server for practical de novo motif discovery. *Nucleic Acids Res.* **35**, W259–W264.
- Causton, H.C., Ren, B., Koh, S.S., Harbison, C.T., Kanin, E., Jennings, E.G., Lee, T.I., True, H.L., Lander, E.S., and Young, R.A. (2001). Remodeling of yeast genome expression in response to environmental changes. *Mol. Biol. Cell* **12**, 323–337.
- Churchman, L.S., and Weissman, J.S. (2011). Nascent transcript sequencing visualizes transcription at nucleotide resolution. *Nature* **469**, 368–373.
- Clos, J., Westwood, J.T., Becker, P.B., Wilson, S., Lambert, K., and Wu, C. (1990). Molecular cloning and expression of a hexameric *Drosophila* heat shock factor subject to negative regulation. *Cell* **63**, 1085–1097.
- Dai, C., Whitesell, L., Rogers, A.B., and Lindquist, S. (2007). Heat shock factor 1 is a powerful multifaceted modifier of carcinogenesis. *Cell* **130**, 1005–1018.
- de Boer, C.G., and Hughes, T.R. (2012). YeTFaSCo: a database of evaluated yeast transcription factor sequence specificities. *Nucleic Acids Res.* **40**, D169–D179.
- Desbarats, L., Gaubatz, S., and Eilers, M. (1996). Discrimination between different E-box-binding proteins at an endogenous target gene of c-myc. *Genes Dev.* **10**, 447–460.
- Eastmond, D.L., and Nelson, H.C.M. (2006). Genome-wide analysis reveals new roles for the activation domains of the *Saccharomyces cerevisiae* heat shock transcription factor (Hsf1) during the transient heat shock response. *J. Biol. Chem.* **281**, 32909–32921.
- Erkine, A.M., Adams, C.C., Diken, T., and Gross, D.S. (1996). Heat shock factor gains access to the yeast HSC82 promoter independently of other sequence-specific factors and antagonizes nucleosomal repression of basal and induced transcription. *Mol. Cell. Biol.* **16**, 7004–7017.
- Fujimoto, M., Takaki, E., Takii, R., Tan, K., Prakasam, R., Hayashida, N., Iemura, S., Natsume, T., and Nakai, A. (2012). RPA assists HSF1 access to nucleosomal DNA by recruiting histone chaperone FACT. *Mol. Cell* **48**, 182–194.
- Gasch, A.P., Spellman, P.T., Kao, C.M., Carmel-Harel, O., Eisen, M.B., Storz, G., Botstein, D., and Brown, P.O. (2000). Genomic expression programs in the response of yeast cells to environmental changes. *Mol. Biol. Cell* **11**, 4241–4257.
- Geiler-Samerotte, K.A., Dion, M.F., Budnik, B.A., Wang, S.M., Hartl, D.L., and Drummond, D.A. (2011). Misfolded proteins impose a dosage-dependent fitness cost and trigger a cytosolic unfolded protein response in yeast. *Proc. Natl. Acad. Sci. U S A* **108**, 680–685.
- Glover, J.R., and Lindquist, S. (1998). Hsp104, Hsp70, and Hsp40: a novel chaperone system that rescues previously aggregated proteins. *Cell* **94**, 73–82.
- Görner, W., Durchschlag, E., Martinez-Pastor, M.T., Estruch, F., Ammerer, G., Hamilton, B., Ruis, H., and Schüller, C. (1998). Nuclear localization of the C2H2 zinc finger protein Msn2p is regulated by stress and protein kinase A activity. *Genes Dev.* **12**, 586–597.
- Gross, D.S., Adams, C.C., Lee, S., and Stentz, B. (1993). A critical role for heat shock transcription factor in establishing a nucleosome-free region over the TATA-initiation site of the yeast HSP82 heat shock gene. *EMBO J.* **12**, 3931–3945.
- Hahn, J.-S., Hu, Z., Thiele, D.J., and Iyer, V.R. (2004). Genome-wide analysis of the biology of stress responses through heat shock transcription factor. *Mol. Cell. Biol.* **24**, 5249–5256.
- Hao, N., and O’Shea, E.K. (2011). Signal-dependent dynamics of transcription factor translocation controls gene expression. *Nat. Struct. Mol. Biol.* **19**, 31–39.
- Hartl, F.U., Bracher, A., and Hayer-Hartl, M. (2011). Molecular chaperones in protein folding and proteostasis. *Nature* **475**, 324–332.
- Haruki, H., Nishikawa, J., and Laemmli, U.K. (2008). The anchor-away technique: rapid, conditional establishment of yeast mutant phenotypes. *Mol. Cell* **31**, 925–932.
- Jakobsen, B.K., and Pelham, H.R. (1988). Constitutive binding of yeast heat shock factor to DNA in vivo. *Mol. Cell. Biol.* **8**, 5040–5042.
- Jakobsen, B.K., and Pelham, H.R. (1991). A conserved heptapeptide restrains the activity of the yeast heat shock transcription factor. *EMBO J.* **10**, 369–375.
- Kaganovich, D., Kopito, R., and Frydman, J. (2008). Misfolded proteins partition between two distinct quality control compartments. *Nature* **454**, 1088–1095.
- Lee, T.I., Rinaldi, N.J., Robert, F., Odom, D.T., Bar-Joseph, Z., Gerber, G.K., Hannett, N.M., Harbison, C.T., Thompson, C.M., Simon, I., et al. (2002).

- Transcriptional regulatory networks in *Saccharomyces cerevisiae*. *Science* 298, 799–804.
- Liu, X.D., Liu, P.C.C., Santoro, N., and Thiele, D.J. (1997). Conservation of a stress response: human heat shock transcription factors functionally substitute for yeast HSF. *EMBO J.* 16, 6466–6477.
- Mahat, D.B., Salamanca, H.H., Duarte, F.M., Danko, C.G., and Lis, J.T. (2016). Mammalian heat shock response and mechanisms underlying its genome-wide transcriptional regulation. *Mol. Cell* 62, 63–78.
- McIsaac, R.S., Silverman, S.J., McClean, M.N., Gibney, P.A., Macinskis, J., Hickman, M.J., Pettit, A.A., and Botstein, D. (2011). Fast-acting and nearly gratuitous induction of gene expression and protein depletion in *Saccharomyces cerevisiae*. *Mol. Biol. Cell* 22, 4447–4459.
- McMillan, D.R., Xiao, X., Shao, L., Graves, K., and Benjamin, I.J. (1998). Targeted disruption of heat shock transcription factor 1 abolishes thermotolerance and protection against heat-inducible apoptosis. *J. Biol. Chem.* 273, 7523–7528.
- Mendillo, M.L., Santagata, S., Koeva, M., Bell, G.W., Hu, R., Tamimi, R.M., Fraenkel, E., Ince, T.A., Whitesell, L., and Lindquist, S. (2012). HSF1 drives a transcriptional program distinct from heat shock to support highly malignant human cancers. *Cell* 150, 549–562.
- Morano, K.A., Santoro, N., Koch, K.A., and Thiele, D.J. (1999). A trans-activation domain in yeast heat shock transcription factor is essential for cell cycle progression during stress. *Mol. Cell. Biol.* 19, 402–411.
- Nicholls, S., Leach, M.D., Priest, C.L., and Brown, A.J.P. (2009). Role of the heat shock transcription factor, Hsf1, in a major fungal pathogen that is obligately associated with warm-blooded animals. *Mol. Microbiol.* 74, 844–861.
- Rabindran, S.K., Giorgi, G., Clos, J., and Wu, C. (1991). Molecular cloning and expression of a human heat shock factor, HSF1. *Proc. Natl. Acad. Sci. U S A* 88, 6906–6910.
- Richter, K., Haslbeck, M., and Buchner, J. (2010). The heat shock response: life on the verge of death. *Mol. Cell* 40, 253–266.
- Sakurai, H., and Ota, A. (2011). Regulation of chaperone gene expression by heat shock transcription factor in *Saccharomyces cerevisiae*: importance in normal cell growth, stress resistance, and longevity. *FEBS Lett.* 585, 2744–2748.
- Sarge, K.D., Murphy, S.P., and Morimoto, R.I. (1993). Activation of heat shock gene transcription by heat shock factor 1 involves oligomerization, acquisition of DNA-binding activity, and nuclear localization and can occur in the absence of stress. *Mol. Cell. Biol.* 13, 1392–1407.
- Scharf, K.D., Rose, S., Zott, W., Schöfl, F., Nover, L., and Schöff, F. (1990). Three tomato genes code for heat stress transcription factors with a region of remarkable homology to the DNA-binding domain of the yeast HSF. *EMBO J.* 9, 4495–4501.
- Schmitt, A.P., and McEntee, K. (1996). Msn2p, a zinc finger DNA-binding protein, is the transcriptional activator of the multistress response in *Saccharomyces cerevisiae*. *Proc. Natl. Acad. Sci. U S A* 93, 5777–5782.
- Smith, A., Ward, M.P., and Garrett, S. (1998). Yeast PKA represses Msn2p/Msn4p-dependent gene expression to regulate growth, stress response and glycogen accumulation. *EMBO J.* 17, 3556–3564.
- Sorger, P.K., and Pelham, H.R. (1987). Purification and characterization of a heat-shock element binding protein from yeast. *EMBO J.* 6, 3035–3041.
- Sorger, P.K., and Pelham, H.R. (1988). Yeast heat shock factor is an essential DNA-binding protein that exhibits temperature-dependent phosphorylation. *Cell* 54, 855–864.
- Tang, Z., Dai, S., He, Y., Doty, R.A., Shultz, L.D., Sampson, S.B., and Dai, C. (2015). MEK guards proteome stability and inhibits tumor-suppressive amyloidogenesis via HSF1. *Cell* 160, 729–744.
- Thevelein, J.M., and de Winde, J.H. (1999). Novel sensing mechanisms and targets for the cAMP-protein kinase A pathway in the yeast *Saccharomyces cerevisiae*. *Mol. Microbiol.* 33, 904–918.
- Torres, F.A.G., and Bonner, J.J. (1995). Genetic identification of the site of DNA contact in the yeast heat shock transcription factor. *Mol. Cell. Biol.* 15, 5063–5070.
- Treger, J.M., Schmitt, A.P., Simon, J.R., and McEntee, K. (1998). Transcriptional factor mutations reveal regulatory complexities of heat shock and newly identified stress genes in *Saccharomyces cerevisiae*. *J. Biol. Chem.* 273, 26875–26879.
- Trinklein, N.D., Murray, J.I., Hartman, S.J., Botstein, D., and Myers, R.M. (2004). The role of heat shock transcription factor 1 in the genome-wide regulation of the mammalian heat shock response. *Mol. Biol. Cell* 15, 1254–1261.
- Wu, C. (1995). Heat shock transcription factors: structure and regulation. *Annu. Rev. Cell Dev. Biol.* 11, 441–469.
- Zarzov, P., Boucherie, H., and Mann, C. (1997). A yeast heat shock transcription factor (Hsf1) mutant is defective in both Hsc82/Hsp82 synthesis and spindle pole body duplication. *J. Cell Sci.* 110, 1879–1891.
- Zhang, Y., Huang, L., Zhang, J., Moskophidis, D., and Mivechi, N.F. (2002). Targeted disruption of hsf1 leads to lack of thermotolerance and defines tissue-specific regulation for stress-inducible Hsp molecular chaperones. *J. Cell. Biochem.* 86, 376–393.

**Supplemental Information**

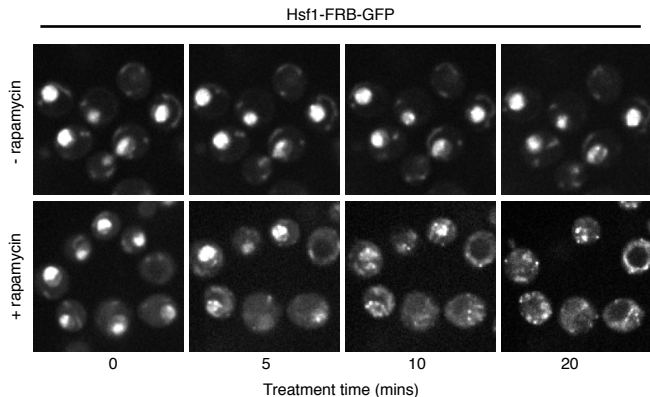
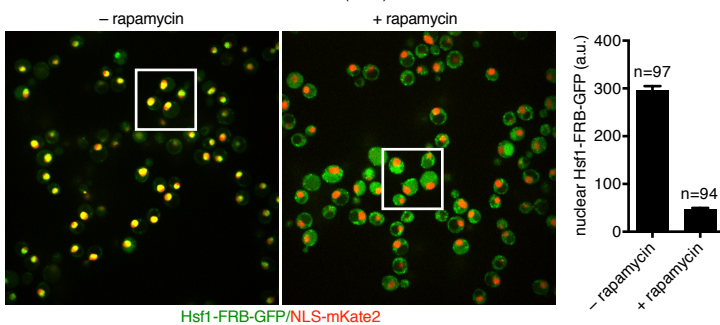
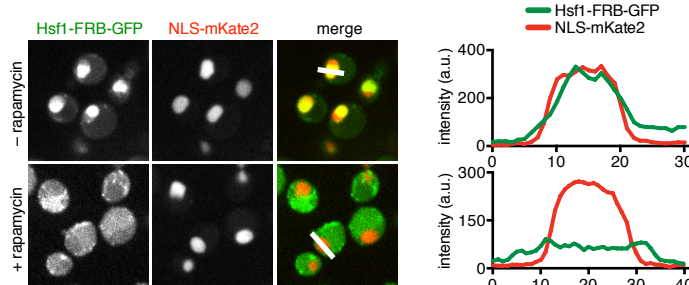
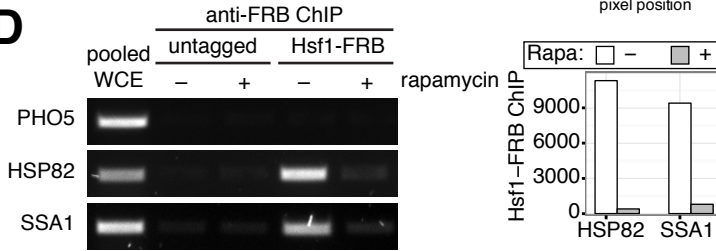
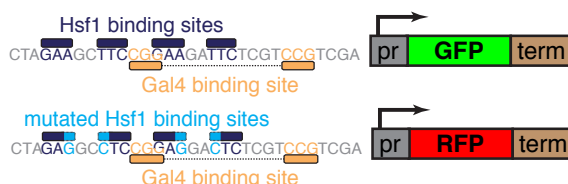
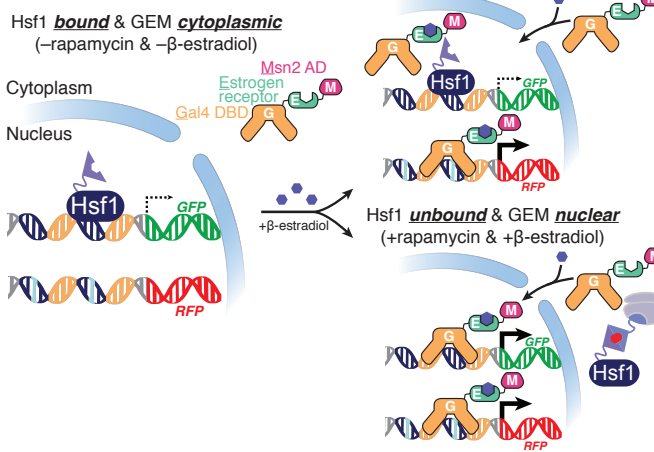
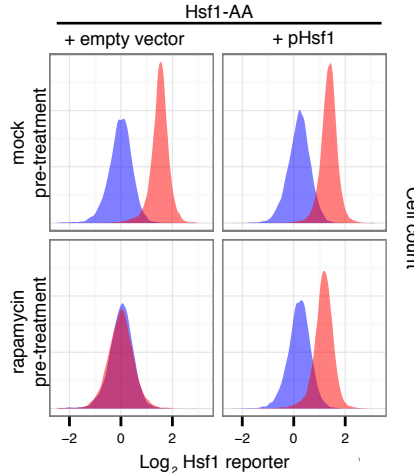
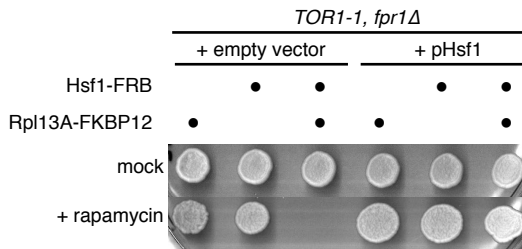
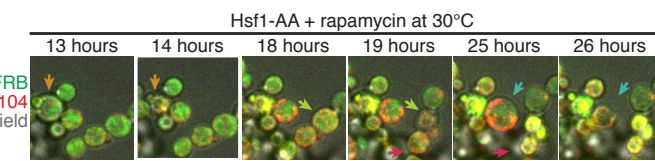
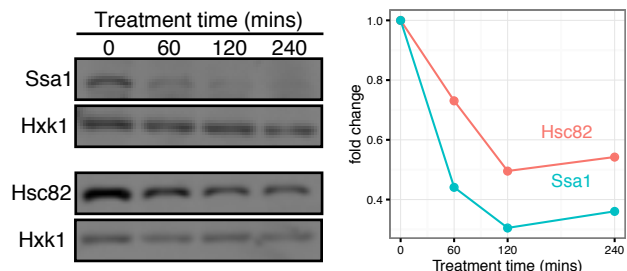
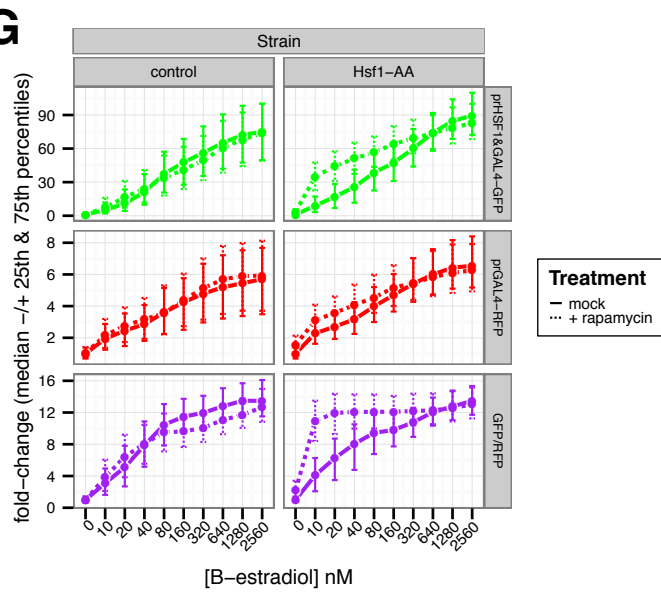
**Defining the Essential Function of Yeast Hsf1  
Reveals a Compact Transcriptional Program  
for Maintaining Eukaryotic Proteostasis**

**Eric J. Solís, Jai P. Pandey, Xu Zheng, Dexter X. Jin, Piyush B. Gupta, Edoardo M. Airoldi, David Pincus, and Vladimir Denic**

## **SUPPLEMENTARY INFORMATION**

**Supplementary Figures:**

# Supplementary Figure 1

**A**

**B**

**C**

**D**

**E**

**F**

**H**

**I**

**J**

**K**

**G**


**Supplementary Figure 1, Related to Figure 1: Validation of Hsf1 Anchor Away as a tool for acute Hsf1 inactivation.**

**(A)** Representative images from confocal micrograph time sequences of Hsf1-AA cells with endogenous Hsf1-FRB-GFP treated with rapamycin at 30°C or left untreated for the indicated times. **(B)** Left: Representative confocal micrographs of merged GFP and mKate2 fluorescence in Hsf1-AA cells co-expressing Hsf1-FRB-GFP and NLS-mKate2 after treatment with 1 $\mu$ M rapamycin for 15 minutes at 30°C or mock treatment. Right: Average of maximal GFP fluorescence in arbitrary units (a.u.) within mKate2-defined nuclei after background subtraction. n corresponds to the number of cells and error bars represent the standard error of the mean. **(C)** Left: Zoomed image of cells boxed in part (B) with the single channel images shown for comparison. Right: One-dimensional GFP and mKate2 fluorescence profiles along the white lines in the images on the left. **(D)** Left: Lysates were prepared from the indicated strains after treatment in the presence or absence of rapamycin for 15 minutes and chromatin was immunoprecipitated using an anti-FRB antibody. Pooled whole cell extracts (WCE) and each IP sample were analyzed by PCR with primers designed to amplify the promoter of *PHO5* (control), *SSA1* (Hsp70) and *HSP82* (Hsp90). Right: Quantification of Hsf1-FRB binding to *HSC82* and *SSA2* promoters in the absence and presence of rapamycin. To remove non-specific signal, we subtracted from the Hsf1-FRB values the band intensity of the identically-treated untagged-Hsf1 IP. **(E)** Top: Schematic and sequence of the overlapping Hsf1 and Gal4 binding sites (dark blue and orange, respectively) embedded in a *CYC1* minimal promoter (pr) driving expression of a GFP gene with the *ACT1* terminator (term). Bottom: mKATE (RFP) version of the reporter above but with selective ablation of Hsf1 binding sites (mutations shown in light blue). **(F)** Schematic of the Hsf1 DNA-binding competition assay. Hsf1-AA cells expressing the two reporters in (E) at genomic loci, as well as a chimeric transcription factor comprising the Gal4 DNA binding domain, the Estrogen-binding domain, and the Msn2 activation domain (referred to as GEM). Treating cells with  $\beta$ -estradiol should cause a dose-dependent accumulation of GEM in the nucleus (McIsaac et al., 2011). (Top right) Bound Hsf1 occludes Gal4 binding sites in the GFP promoter restricting GEM access at low  $\beta$ -estradiol concentrations relative to the accessibility of the RFP promoter. (Bottom right) Rapamycin treatment of Hsf1-AA cells prevents Hsf1 binding to the GFP promoter resulting in enhanced GEM access to the GFP promoter at low  $\beta$ -estradiol concentrations. **(G)** The two-color reporter described in (E) and the  $\beta$ -estradiol regulated GEM transcription factor described in (F) were expressed in Hsf1-AA cells or isogenic control cells with endogenous Hsf1 (untagged). Cells were treated with 10 $\mu$ M rapamycin or mock-treated along with the indicated concentration of  $\beta$ -estradiol for 90' at 30°C and then analyzed by flow cytometry. Plots in the top and middle panels show the size-normalized median fluorescence from ~10,000 single cells for each condition (with error bars showing the 25<sup>th</sup> and 75<sup>th</sup> percentiles of the single-cell distributions) after raw values were normalized by dividing by the median of the mock treated, no- $\beta$ -estradiol sample for each strain. Since the two promoters drive different fluorescent proteins the raw fold changes for GFP and RFP at a given concentration of  $\beta$ -estradiol are not directly reflective of the promoter accessibility (*i.e.*, a larger GFP vs. RFP fold change

does not mean the GFP promoter is more accessible). However, by comparing the GFP/RFP ratio in single-cells across  $\beta$ -estradiol concentrations (bottom panels) the relative accessibility of the two promoters can be determined: similar GEM binding to both promoters will induce a similar GFP/RFP ratio across  $\beta$ -estradiol concentrations, while occlusion of GEM by Hsf1 binding in the GFP promoter will result in a lower GFP/RFP ratio at lower  $\beta$ -estradiol concentration compared to higher concentrations where nuclear GEM abundance should be sufficient to out compete Hsf1 for binding to the dual promoter. **(H)** Hsf1-AA cells with indicated plasmids and Hsf1 reporter—GFP expressed from a minimal promoter containing four engineered Hsf1-binding sites and mKate (RFP) constitutively expressed from the *TEF2* promoter—were grown logarithmically at 30°C prior to pre-treatment with rapamycin (10' at 30°C) or mock pre-treatment. This was followed by heat shock (39°C for 30') or control treatment (30°C) and, finally, cells were analyzed by flow cytometry. Shown are cell plots of Hsf1 reporter activity, which we defined as the  $\log_2$  ratio of GFP to RFP fluorescence normalized to the median fluorescence of cells with empty vector after mock pre-treatment and control treatment. **(I)** Rapamycin-resistant *TOR1-1*,  $\Delta fpr1$  cells with indicated plasmids and endogenous untagged Hsf1 and Rpl13A or C-terminally tagged with FRB and FKBP12, respectively and as indicated, were spotted onto rapamycin or mock (carrier-only) plates. Shown are images of plates incubated at 30°C for 3 days. **(J)** Representative images from a epifluorescence micrograph time sequence of Hsf1-AA cells with endogenous Hsf1-FRB-GFP and Hsp104-RFP treated with rapamycin at 30°C for the indicated times. Arrows point at cells that lysed between adjacent time points. **(K)** Whole cell lysates prepared from Hsf1-AA cells growing logarithmically at 30°C after treatment with rapamycin for the indicated times were resolved by SDS-page and analyzed by Western blotting using anti-Hsc82 (Hsp90), anti-Ssa1 (Hsp70) and anti-Hxk1 antibodies. Left: A representative fluorescence micrograph of a blot from one of the two technical replicates. Right: Quantitation of Hsc82 and Ssa1 levels relative to the Hxk1 level at each timepoint was determined using ImageQuant after establishing the baseline for each band intensity using the rolling ball parameter. Plotted are average fold changes from two technical replicates relative to untreated cells at the beginning of the timecourse.



**Supplementary Figure 2, Related to Figure 2: Defining Hsf1 targets by statistical analyses of Hsf1 promoter binding and transcription/mRNA changes induced by Hsf1 Anchor Away.**

(A) Hsf1-AA cells growing logarithmically at 30°C were analyzed NET-seq immediately prior to and after 15', 30' and 60' of rapamycin treatment. Shown are gene scatter plots comparing transcription ( $\log_2$  read fragments per-kilobase per million reads, or FPKM) between adjacent time points (Left: control vs. 15'; Middle: 15' vs. 30'; Right: 30' vs. 60'). Genes defined as significantly different between control and 15' time points ( $p < 10^{-4}$ ) are indicated in blue with 95% confidence intervals (error bars) in all three panels.

Global summary statistics (top left in each panel) were computed based on transcription changes for each detected gene. (B) Hsf1-AA cells growing logarithmically at 30°C (control), and after treatment with rapamycin for 60', were analyzed by RNA-seq. Left: Gene ranking by mRNA abundance change induced by treatment. Genes below and above the 1<sup>st</sup> and 99<sup>th</sup> percentiles (dashed lines), respectively, were defined as significantly Hsf1-dependent. Genes defined by NET-seq analysis were color-coded blue if they were also defined by RNA-seq analysis and red if they were not. Right: Gene histogram of fold-changes induced by treatment.

(C) Time-course of HDG transcription changes induced by rapamycin treatment at 30°C. (D) Gene scatter plot of transcription versus mRNA changes induced by treatment with rapamycin for 15' and 60', respectively. Linear regression fits and  $R^2$  values are shown for genes with significant changes by NET-seq and RNA-seq, NET-seq alone, or neither, as defined by statistical tests described in Experimental Procedures. (E) CDF of 95% confidence interval widths for transcription of HDGs or all other genes based on NET-seq analysis of indicated samples. For each data set, the y-axis corresponds to the proportion of HDGs or all other genes with a 95% C.I. width less than or equal to the x-axis value. P-values are for the Wilcoxon rank-sum test for equal C.I. width distributions between HDGs and all other genes. ns: not significant.

(F) CDF of standard deviations of transcription for HDGs or all other genes based on NET-seq analysis of indicated samples. The y-axis corresponds to the proportion of HDGs or all other genes with a standard deviation (SD) less than or equal to the x-axis value. P-values are for the Wilcoxon rank-sum test for equal distributions of SDs for HDGs and other genes for the same condition.

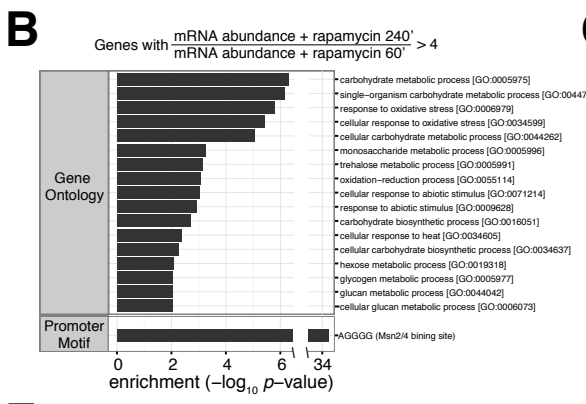
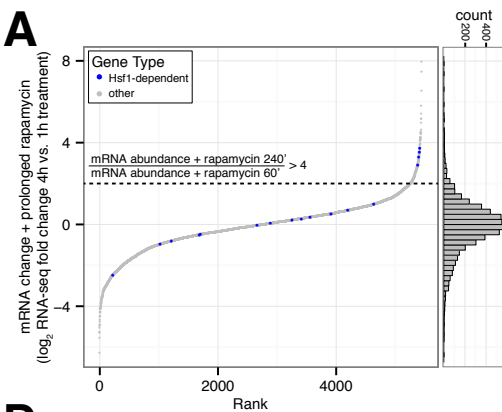
(G) Gene scatter plot of standard deviation (SD) of transcription measurements ( $\log_2$  FPKM) for each gene after rapamycin treatment (for 15', 30' and 60') versus transcription of that gene ( $\log_2$  FPKM) in untreated cells. HDGs are indicated in blue and a local smoothed regression fit for all genes is in black. Marginal histograms for SDs and transcription of all genes are right and above, respectively.

(H) Hsf1-FLAG-V5 cells growing logarithmically at 30°C were analyzed by ChIP-seq. Shown are distributions of ChIP-seq reads at the HDG loci. (I) Gene scatter plot comparing Hsf1 target transcriptional decline (defined by NET-seq fold-change after 15' rapamycin treatment relative to control for Hsf1-AA cells) with Hsf1 binding to target promoters (defined by ChIP-seq analysis of Hsf1-FLAG-V5 cells). HDGs are shown in blue, while the remaining Hsf1 targets defined by ChIP-seq are gray. Linear regression and  $R^2$  values for each gene set are indicated.

(J) Bioinformatic analysis of Hsf1 targets defined by ChIP-seq, NET-seq and RNA-seq, individually or the intersection of genes defined by

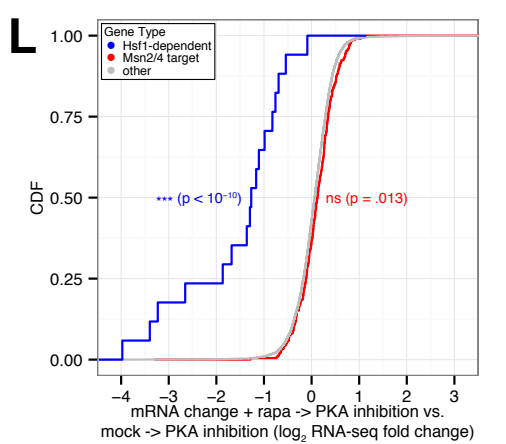
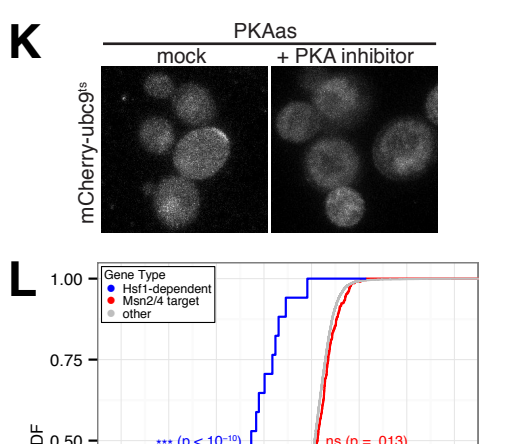
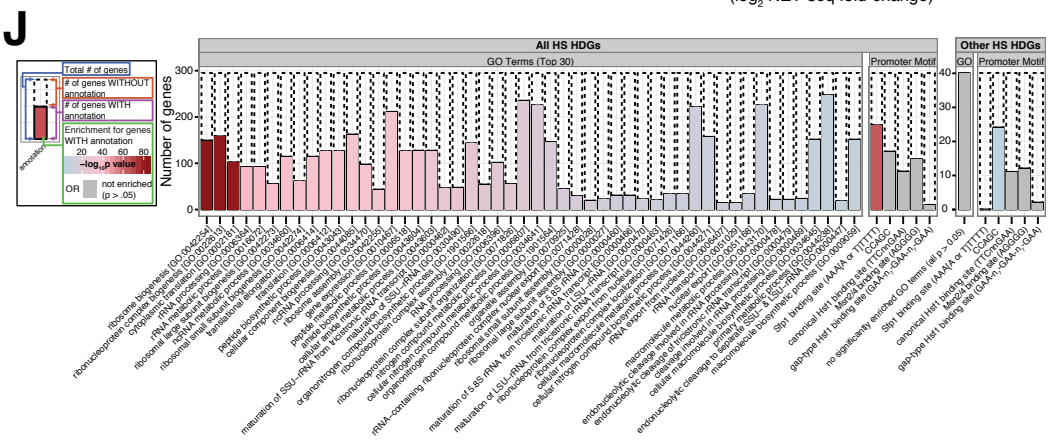
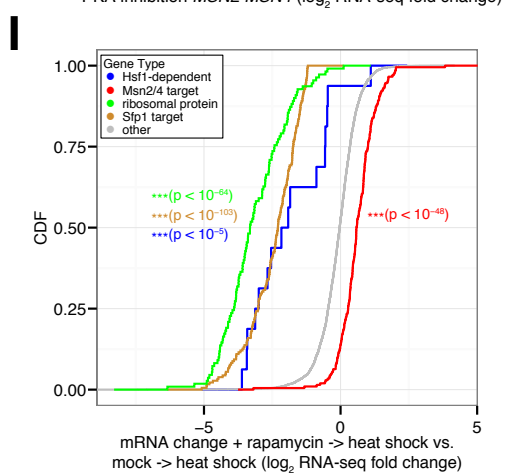
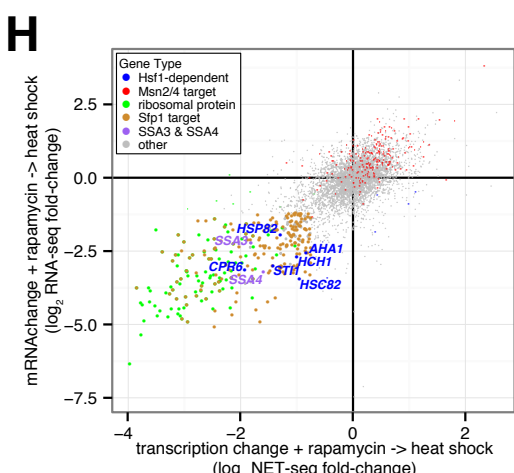
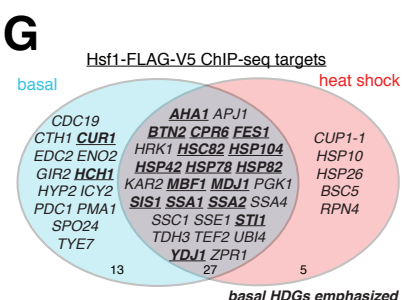
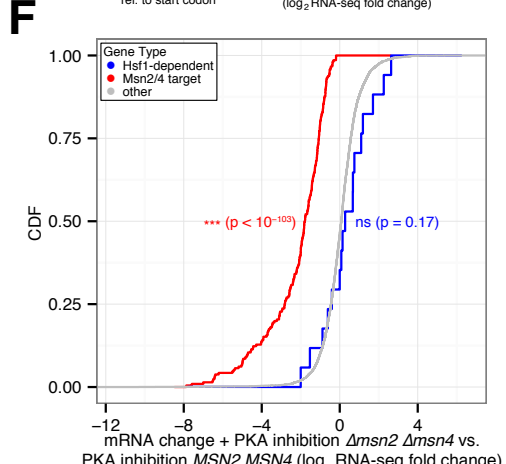
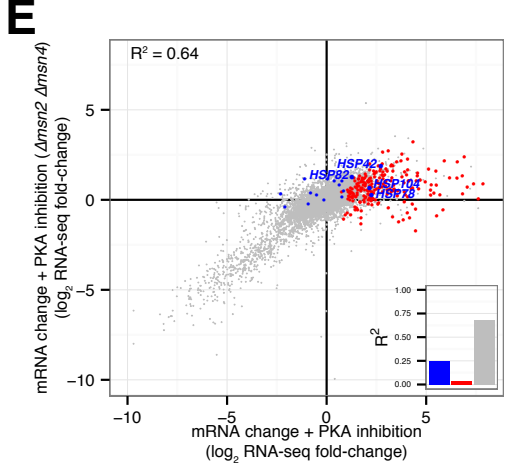
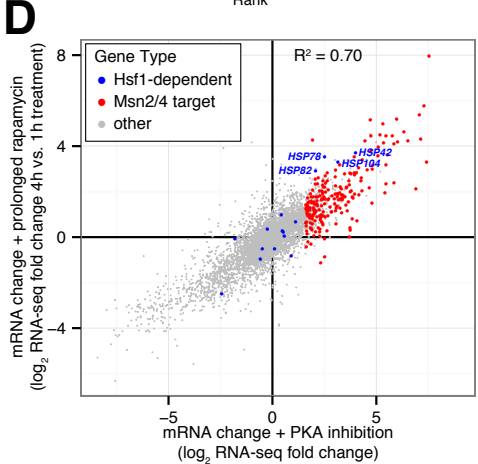
the indicated combinations of techniques. The height of the solid bars indicates the number of genes with the given annotation (GO term or promoter motif), while the height of dashed bars indicates the number of remaining genes lacking the annotation. The fill color indicates the significance of the enrichment for the annotated Hsf1 targets versus other genes (p-values for GO terms are corrected for multiple testing using the Holm–Bonferroni method). If no bar is shown for a given GO term in a particular technique category, it was not significantly enriched for Hsf1 targets (p-value > .1).

# Supplementary Figure 3



-750 -500 -250 0 2 4 mRNA change + rapamycin 60 min > 240 min (log<sub>2</sub>RNA-seq fold change)

Binding Site  
Hsf1 Msn2/4



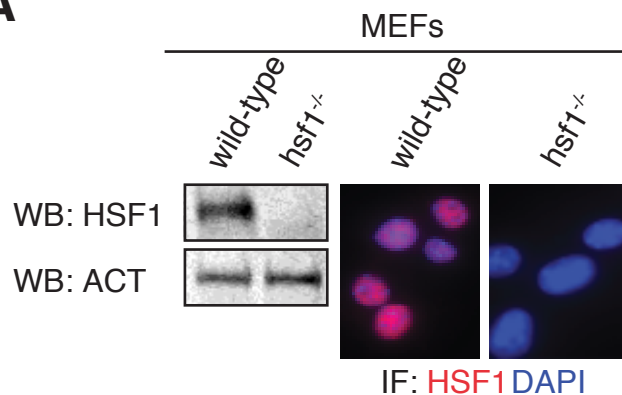
**Supplementary Figure 3, Related to Figure 3: Msn2/4 gene targets are induced by prolonged Hsf1 inactivation, heat shock, and PKA inhibition by chemical genetics.**

**(A)** Hsf1-AA cells were grown logarithmically at 30°C were treated with rapamycin for 60' and 240' then analyzed by RNA-seq. Left: Gene ranking by mRNA abundance change induced by treatment. Genes above the dashed line have a >4-fold increase in mRNA abundance. HDGs are indicated in blue. Right: Gene histogram of fold-changes induced by treatment. **(B)** Bioinformatic analysis of genes with > 4-fold increase in mRNA abundance induced by prolonged rapamycin treatment. Bar lengths indicate the significance level of their enrichment for the given annotation (GO term or promoter motif) (p-values for GO terms corrected for multiple testing using the Holm–Bonferroni method). **(C)** Left: HDG promoter locations of Hsf1 and Msn2/4 binding sites as in Figure 3B. Right: Hsf1-AA cells grown logarithmically at 30°C were treated with rapamycin for 60' or 240' prior to harvesting for RNA-seq analysis. Shown are HDG mRNA changes induced by prolonged rapamycin treatment. **(D)** Gene scatter plot comparing mRNA changes induced by PKA inhibition (see Figure 3D) versus prolonged rapamycin treatment (see Figure 3A). Msn2/4 targets were defined as genes with at least one Msn2/4 promoter binding site (AGGGG) that were in the top 10% of genes induced by PKA inhibition. **(E)** PKAas and PKAas  $\Delta msn2 \Delta msn4$  cells were grown logarithmically at 30°C (control) or treated with 1-NM-PP1 (120' at 30°C) prior to harvesting for RNA-seq analysis. Shown is a gene scatter plot of mRNA changes induced by PKA inhibition in each strain relative to PKAas control. **(F)** Cumulative distribution function (CDF) of mRNA abundance fold-changes induced by PKA inhibition in PKAas  $\Delta msn2 \Delta msn4$  versus PKAas cells in part (E). For each of the three gene types indicated, the y-axis corresponds to the proportion of genes within a gene type with fold-change ratios less than or equal to the corresponding value on the x-axis. P-values are for the Wilcoxon rank-sum test for equal distributions of fold-changes for the indicated gene type versus the distribution of changes for the other two types combined. **(G)** Venn diagram comparing Hsf1 target genes defined by ChIP-seq analysis of Hsf1-FLAG-V5 cells under basal (30°C) and heat shock (39°C) conditions. The names of previously defined HDGs are emphasized. **(H)** Hsf1-AA cells were pretreated with rapamycin or carrier-only (for 15' or 30' at 30°C) and then heat shock (30' at 39°C) prior to harvesting for analysis by NET-seq and RNA-seq. Shown is a gene scatter plot of transcription versus mRNA changes after heat shock induced by pre-treatment with rapamycin for 15' and 30', respectively, relative carrier pretreatment control. Colors denote gene sets and large points correspond to genes with significantly decreased transcription and mRNA abundance, as described in Supplementary Experimental Procedures. **(I)** CDF of mRNA abundance fold-changes induced by heat shock after rapamycin pretreatment versus mock pretreatment in part (H). For each gene set, the y-axis corresponds to the proportion of genes in the set with fold-change ratios less than or equal to the corresponding value on the x-axis. P-values are for the Wilcoxon rank-sum test for equal distributions of fold-changes for that gene set versus the distribution of changes for the other gene types combined. **(J)** Bioinformatic analysis of genes with significant decreases in heat shock transcription and mRNA abundance due to rapamycin treatment in part (H), for all significant genes (left), or other type genes

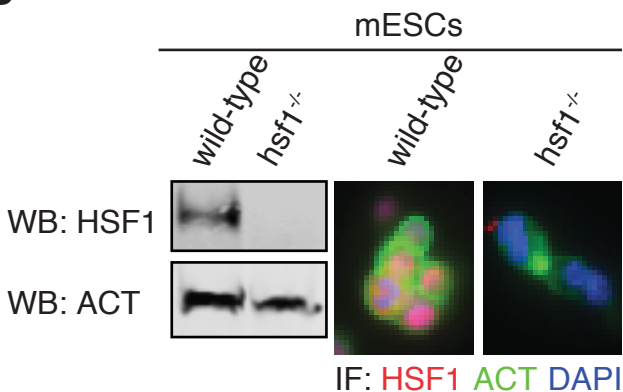
(significant genes that are not HDGs, *SSA3/4*, ribosomal protein genes or *Sfp1* targets), see Supplementary Experimental Procedures for details. Solid bars show the number of heat shock (HS) HDGs genes with the given annotation (GO term or promoter motif) and dashed bars show the number of remaining genes. The fill color indicates the significance level for the enrichment of the annotated HS HDGs versus all genes (p-values for GO terms are corrected for multiple testing using the Holm–Bonferroni method). Note: The CCAGC motif corresponds to the binding sites for Hac1, Swi5, and Ace2. **(K)** Representative confocal micrographs of PKAas cells expressing plasmid-borne mCherry-ubc9<sup>ts</sup> after treatment with PKA inhibitor (1-NM-PP1) or mock (carrier-only) for 180' at 30°C. **(L)** CDF of mRNA abundance fold-changes induced by PKA inhibition after rapamycin pretreatment versus mock pretreatment in Figure 3E. For each gene set, the y-axis corresponds to the proportion of genes within a gene type with fold-change ratios less than or equal to the corresponding value on the x-axis. P-values are for the Wilcoxon rank-sum test for equal distributions of fold-changes for the indicated gene type versus the distribution of changes for the other gene types combined.

# Supplementary Figure 4

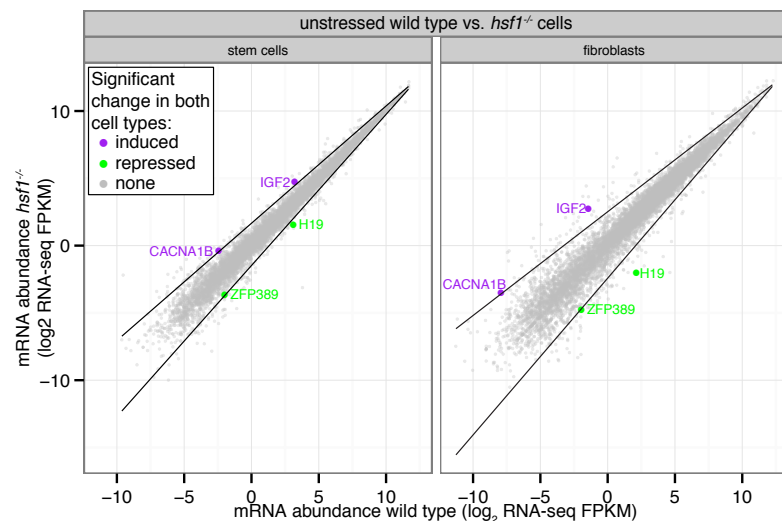
**A**



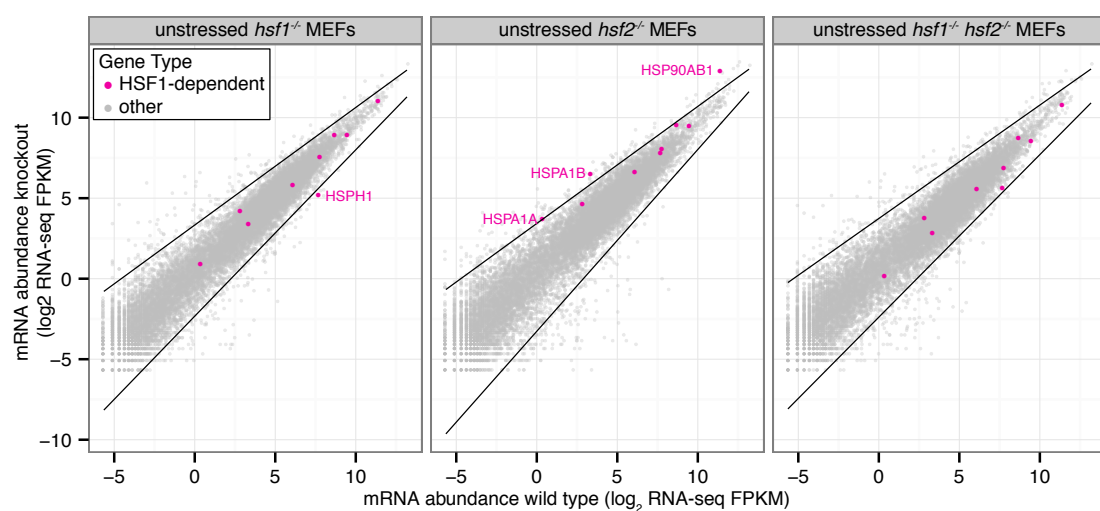
**B**



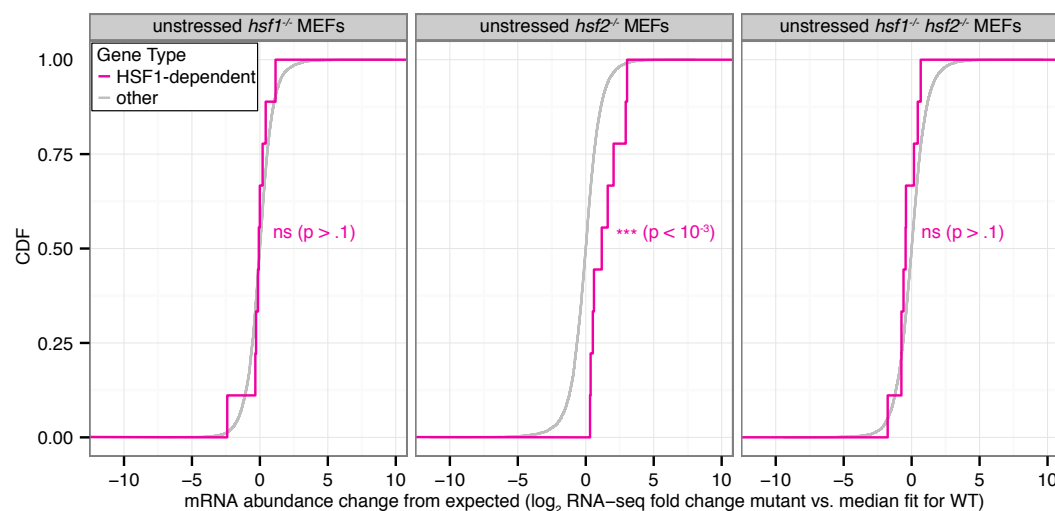
**C**



**D**



**E**



**Supplementary Figure 4, Related to Figure 4: Validation of loss of HSF1 expression in *hsf1*<sup>-/-</sup> MEFs and mESCs, and analysis of HDG expression dependence on HSF1 and HSF2.**

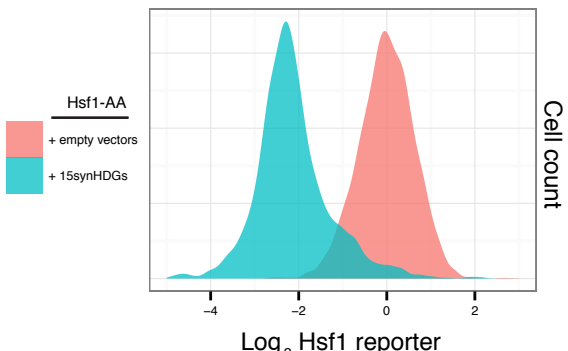
**(A)** Left: Whole cell lysates prepared from indicated MEFs were resolved by SDS-PAGE and analyzed by Western blotting (WB) with anti-Hsf1 and anti-ACT (Actin) antibodies. Right: Indicated MEFs were analyzed by immunofluorescence (IF) with anti-HSF1 antibody (red) and co-stained with DAPI (blue). **(B)** Indicated mESCs were analyzed as in (A), but with additional actin IF staining (green). **(C)** Wild-type (WT) and *hsf1*<sup>-/-</sup> knock out (KO) MEFs and mESCs were cultured at 37°C prior to harvesting for RNA-seq analysis. Shown is a gene scatter plot of mRNA abundances WT and KO cells for each cell type. Dark lines indicate statistical thresholds used to define genes with significant changes in expression (see Experimental Procedures) and genes with significant changes in both cell types are colored. Also indicated are gene names of HSF1-dependent genes (HDGs) defined by additional experiments and analyses (see Figures 4A-C and Experimental Procedures). **(D)** Wild-type (WT), *hsf1*<sup>-/-</sup>, *hsf2*<sup>-/-</sup> and *hsf1*<sup>-/-</sup> *hsf2*<sup>-/-</sup> MEFs were cultured at 37°C and analyzed by RNA-seq. Shown is a gene scatter plot of mRNA abundances in each knock out line against the common wildtype. Dark lines indicate statistical thresholds used to define genes with significant changes in expression (see Experimental Procedures). HDGs are colored pink with only the names of HDGs with significant changes indicated. **(E)** CDF of  $\log_2$  mRNA abundance differences between measured and expected KO gene expression, the latter being derived from a linear regression fit of the median KO mRNA abundance onto wild type mRNA abundance using data from (D). For each mutant, the y-axis corresponds to the proportion of genes in the set with an mRNA abundance difference less than or equal to the corresponding value on the x-axis. P-values are for the Wilcoxon rank-sum test for equal distributions of differences for HDGs versus all other genes.

# Supplementary Figure 5

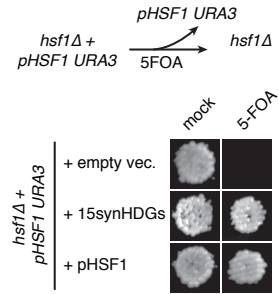
**A**

synHdG open reading frame	synHdG promoter				
	Pr <sub>ADH1</sub>	Pr <sub>CYC1</sub>	Pr <sub>PGK1</sub>	Pr <sub>TDH3</sub>	Pr <sub>TEF1</sub>
(A)	YDJ1			HSC82	SIS1
(B)	FES1		AHA1	STI1	SSA2
(C)	HSP78	MDJ1		CUR1	HSP104
(D)	MBF1	HSP42		BTN2	CPR6

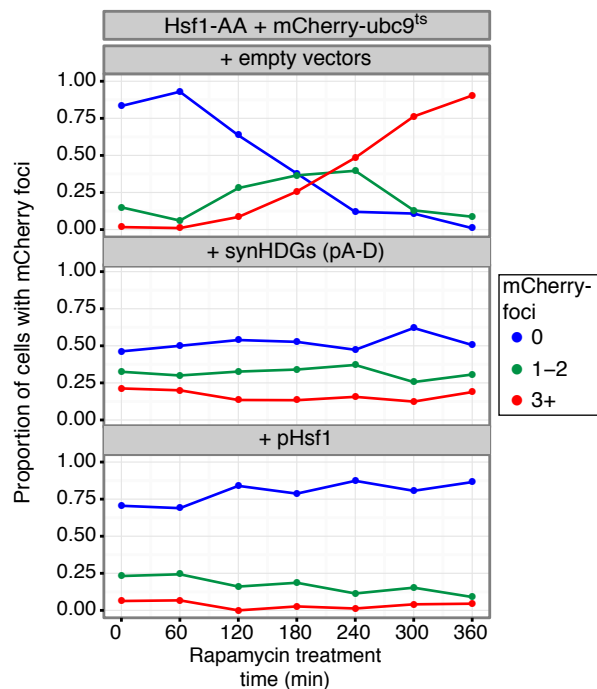
**B**



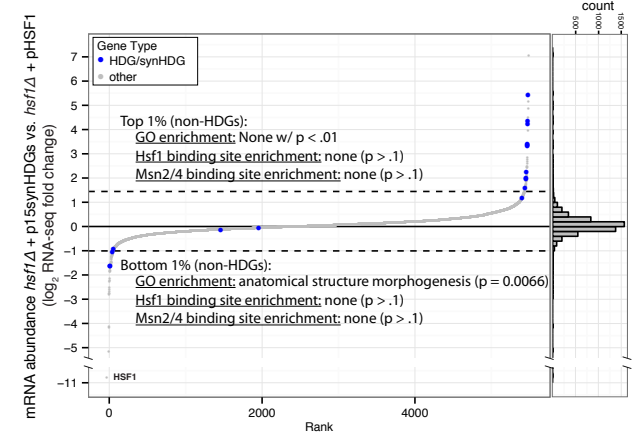
**D**



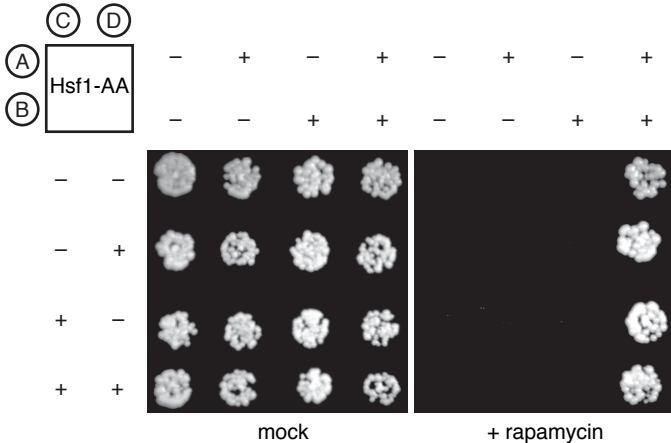
**C**



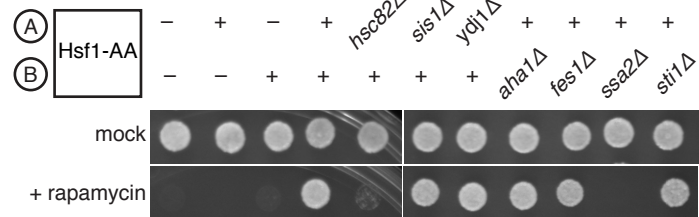
**E**



**F**

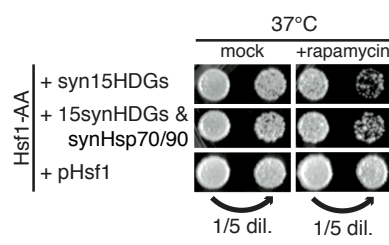


**G**



**H**

**I**



Hsf1-AA + mCherry-ubc9<sup>ts</sup>

	+ empty	+ synHsp90	+ synHsp70	+ synHsp70/90
+ rapamycin	8	6	9	73
% of cells with 0/1-2/3+ mCherry foci	90	90	71	15

**Supplementary Figure 5, Related to Figure 5: Defining the minimal synthetic transcriptional program that bypasses Hsf1's essential function.**

**(A)** ORF and promoter annotation of four synHDG expression plasmids used in this study. Each plasmid is low-copy plasmid in yeast and carries a unique marker gene. **(B)** Hsf1-AA cells with Hsf1 reporter and indicated plasmids were grown logarithmically at 30°C prior to flow cytometry analysis. Shown are cell plots of Hsf1 reporter activity (see Supplementary Figure 1H for details). **(C)** Hsf1-AA cells expressing plasmid-borne mCherry-ubc9<sup>ts</sup> and indicated plasmids were treated with rapamycin for indicated times at 30°C and imaged by epifluorescence microscopy. Blinded images containing at least 100 cells were scored for cells containing either 0/1-2/3+ mCherry foci and the fraction of scored cells plotted. **(D)** Top: Addition of the drug 5-FOA to  $\Delta hsf1$  *ura3*<sup>-</sup> with *URA3*-marked *HSF1* expression plasmid kills URA<sup>+</sup> cells to enable selection of cells that have spontaneously lost the *URA3*-marked plasmid. Bottom: *hsf1* $\Delta$  cells carrying a *URA3*-marked Hsf1 expression plasmid plus non-*URA3* marked expression plasmids for 15synHDGs (plasmids A-D in Figure S4A) or Hsf1 were spotted onto 5-FOA or mock plates. Shown are images of plates incubated for 3 days at 30°C. **(E)** *hsf1* $\Delta$  cells carrying expression plasmids for 15synHDGs or Hsf1 were logarithmically grown at 30°C prior to harvesting for RNA-seq analysis. Left: Gene ranking of mRNA abundance fold-changes for  $\Delta hsf1$  cells expressing plasmid-borne 15synHDGs versus Hsf1. Bioinformatic analysis of non-HDGs in the top and bottom 1% of fold-changes are indicated. Right: Gene histogram of fold-changes for all genes. **(F)** Hsf1-AA cells transformed with indicated plasmid combinations of four synHDG plasmids (plasmids A-D in Figure S4A) and four corresponding empty vectors (-) were spotted onto rapamycin or mock (carrier-only) control plates. Shown are images of plates incubated for 3 days at 30°C. **(G)** Hsf1-AA cells transformed with indicated plasmid combinations (plasmids with individual HDGs deleted are described in the Experimental Procedures) were spotted onto rapamycin or mock (carrier-only) plates. Shown are images of plates incubated for 3 days at 30°C. **(H)** Representative epifluorescence micrographs of Hsf1-AA cells expressing plasmid-borne mCherry-ubc9<sup>ts</sup> and indicated synHsps or empty control were treated with β-estradiol (30') to induce Hsp expression followed by treatment with rapamycin (7 hours). Blinded images containing at least 100 cells were scored for cells containing indicated number of mCherry foci. Percentage of scored cells is shown below micrographs. **(G)** Hsf1-AA cells expressing indicated transgenes were spotted at two concentrations onto rapamycin or mock (carrier-only) plates, which also contained β-estradiol to drive synHsp expression from β-estradiol-dependent promoters (see Experimental Procedures for details). Shown are images of plates incubated at 37°C for 5 days.

**SUPPLEMENTARY TABLES:**

- Table S1: Hsf1-AA NET-seq data, Related to Figure 2.  
Table S2: Yeast RNA-seq data, Related to Figure 2.  
Table S3: Hsf1-FLAG-V5 ChIP-seq data, Related to Figure 2.  
Table S4: Mammalian RNA-seq data, Related to Figure 4.

Table S5: Yeast strains and cell lines, Related to Figure 5.

<b>Yeast Strain</b>	<b>Genotype</b>
W303	<i>leu2-3,112 trp1-1 can1-100 ura3-1 ade2-1 his3-11,15</i>
VDY1667	W303 MAT <sub>a</sub> TPK1/2/3/as TOR1-1(S1972I) <i>fpr1Δ::NATMX Pr<sub>TEF2</sub>-mKATE2-URA3-4xHSE-Pr<sub>CYC1</sub>-EmGFP RPL13A-2xFKBP12-TRP1</i>
VDY1852	W303 MAT <sub>a</sub> TPK1/2/3/as TOR1-1(S1972I) <i>fpr1Δ::NATMX Pr<sub>TEF2</sub>-mKATE2-URA3-4xHSE-Pr<sub>CYC1</sub>-EmGFP RPL13A-2xFKBP12-TRP1 HSF1-FRB-HIS3MX6</i>
VDY1853	W303 MAT <sub>a</sub> TPK1/2/3/as TOR1-1(S1972I) <i>fpr1Δ::NATMX Pr<sub>TEF2</sub>-mKATE2-URA3-4xHSE-Pr<sub>CYC1</sub>-EmGFP HSF1-FRB-HIS3MX6</i>
VDY1874	W303 MAT <sub>a</sub> TPK1/2/3/as TOR1-1(S1972I) <i>fpr1Δ::NATMX RPL13A-2xFKBP12-TRP1</i>
VDY1896	W303 MAT <sub>a</sub> TPK1/2/3/as TOR1-1(S1972I) <i>fpr1Δ::NATMX RPL13A-2xFKBP12-TRP1 HSF1-FRB-HIS3MX6</i>
VDY1877	W303 MAT <sub>a</sub> TPK1/2/3/as TOR1-1(S1972I) <i>fpr1Δ::NATMX RPL13A-2xFKBP12-TRP1 HSF1-FRB-GFP-HIS3MX</i>
VDY2130	W303 MAT <sub>a</sub> TPK1/2/3/as TOR1-1(S1972I) <i>fpr1Δ::NATMX RPL13A-2xFKBP12-TRP1 HSF1-FRB-HIS3MX HSP104-mCLOVER-KANMX</i>
VDY2254	W303 MAT <sub>a</sub> TPK1/2/3/as TOR1-1(S1972I) <i>fpr1Δ::NATMX Pr<sub>TEF2</sub>-mKATE2-URA3-4xHSE-Pr<sub>CYC1</sub>-EmGFP RPL13A-2xFKBP12-TRP1 HSF1-FRB-HIS3MX6RPB3-FLAG-KANMX</i>
VDY2367	W303 MAT <sub>a</sub> TPK1/2/3/as TOR1-1(S1972I) <i>fpr1Δ::NATMX Pr<sub>TEF2</sub>-mKATE2-URA3-4xHSE-Pr<sub>CYC1</sub>-EmGFP RPL13A-2xFKBP12-TRP1 HSF1-FRB-KANMX</i>
VDY2578	W303 MAT <sub>a</sub> TPK1/2/3/as TOR1-1(S1972I) <i>fpr1Δ::NATMX ura3-1 RPL13A-2xFKBP12-TRP1 HSF1-FRB-KANMX</i>
VDY2595	W303 MAT <sub>a</sub> TPK1/2/3/as TOR1-1(S1972I) <i>fpr1Δ::NATMX Pr<sub>TEF2</sub>-mKATE2-ura3-1-4xHSE-Pr<sub>CYC1</sub>-EmGFP RPL13A-2xFKBP12-TRP1HSF1-FRB-KANMX</i>
VDY2688	W303 MAT <sub>a</sub> <i>hsf1Δ::KAN HSF1-3xFLAG-V5::TRP1</i>
VDY466	W303 MAT <sub>a</sub> TPK1/2/3as ADE2
VDY488	W303 MAT <sub>a</sub> TPK1/2/3as ADE2 <i>msn4Δ::TRP1 msn2Δ::NATMX</i> W303 MAT <sub>a</sub> TPK1/2/3/as TOR1-1(S1972I) <i>fpr1Δ::NATMX RPL13A-2xFKBP12-TRP1 HSF1-FRB-GFP-HIS3MXPr<sub>TDH3</sub>-NLS-mKATE2::LEU2</i>
DPY813	

<b>Cell Line</b>	<b>Description</b>
mDP1	CBA316 (Immortalized mEFs)
mDP4	ES Cells ES129
mDP10	mEF <i>hsf1-/-</i> (using CRISPR/Cas9) derived from mDP1
mDP11	mES <i>hsf1-/-</i> (using CRISPR/Cas9) derived from mDP4
mDP12	mEF <i>hsf2-/-</i> (using CRISPR/Cas9) derived from mDP1
mDP13	mEF <i>hsf1-/- hsf2-/-</i> (using CRISPR/Cas9) derived from mDP10

## Supplemental Experimental Procedures

### Yeast strains and plasmids.

Yeast strains used in this work are described in Table S5. Plasmids used are detailed below:

Plasmid	Construct
pNH605	Sfil – Pr <sub>Sc LEU2</sub> – Cg LEU2 – multiple cloning site – 3'-UTR <sub>Sc LEU2</sub> – Sfil
pRS412	ADE2 CEN/ARS
pRS413	HIS3 CEN/ARS
pRS415	LEU2 CEN/ARS
pRS416	URA3 CEN/ARS
pVD380	pESC Pr <sub>GAL1</sub> -mCherry-UBC9wt LEU2
pVD381	pESC Pr <sub>GAL1</sub> -mCherry-ubc9ts LEU2
pVD476	pRS413 HSF1 (promoter - ORF - 3'-UTR)
pVD565	pRS412 HSF1
pVD570	pRS412 Pr <sub>ADH1</sub> -YDJ1 (ORF and 3'-UTR) – Pr <sub>TDH3</sub> -HSC82 (ORF and 3'-UTR) – Pr <sub>TEF1</sub> -SIS1 (ORF and 3'-UTR)
pVD576	pRS415 Pr <sub>PGK1</sub> -AHA1 (ORF and 3'-UTR) – Pr <sub>ADH1</sub> -FES1 (ORF and 3'-UTR) – Pr <sub>TEF1</sub> -SSA2 (ORF and 3'-UTR) – Pr <sub>TDH3</sub> -STI1 (ORF and 3'-UTR)
pVD577	pRS412 Pr <sub>TDH3</sub> -CUR1 (ORF and 3'-UTR) – Pr <sub>ADH1</sub> -HSP78 (ORF and 3'-UTR) – Pr <sub>TEF1</sub> -HSP104 (ORF and 3'-UTR) – Pr <sub>CYC1</sub> -MDJ1 (ORF and 3'-UTR)
pVD578	pRS413 Pr <sub>TDH3</sub> -BTN2 (ORF and 3'-UTR) – Pr <sub>TEF1</sub> -CPR6 (ORF and 3'-UTR) – Pr <sub>CYC1</sub> -HSP42 (ORF and 3'-UTR) – Pr <sub>ADH1</sub> -MBF1 (ORF and 3'-UTR)
pVD579	pRS412 ade2Δ::HPHMX
pVD580	pRS412 ade2Δ::HPHMX Pr <sub>ADH1</sub> -YDJ1 (ORF and 3'-UTR) – Pr <sub>TDH3</sub> -HSC82 (ORF and 3'-UTR) – Pr <sub>TEF1</sub> -SIS1 (ORF and 3'-UTR)
pVD632	pESC Pr <sub>GAL1</sub> -mCherry-ubc9ts URA3
pVD783	pRS416 Pr <sub>ACT1</sub> -Z <sub>4</sub> EV-term <sub>ADH1</sub> – 6xZ <sub>4</sub> BS-Pr <sub>CYC1</sub> -term <sub>ADH1</sub>
pVD784	pRS416 Pr <sub>ACT1</sub> -Z <sub>4</sub> EV-term <sub>ADH1</sub> – 6xZ <sub>4</sub> BS-Pr <sub>CYC1</sub> -SSA2 (ORF and 3'-UTR)-term <sub>ADH1</sub>
pVD785	pRS416 Pr <sub>ACT1</sub> -Z <sub>4</sub> EV-term <sub>ADH1</sub> – 6xZ <sub>4</sub> BS-Pr <sub>CYC1</sub> -HSC82 (ORF and 3'-UTR)-term <sub>ADH1</sub>
pVD786	pRS416 6xZ <sub>4</sub> BS-Pr <sub>CYC1</sub> -HSC82 (ORF and 3'-UTR) – Pr <sub>ACT1</sub> -Z <sub>4</sub> EV-term <sub>ADH1</sub> – 6xZ <sub>4</sub> BS-Pr <sub>CYC1</sub> -SSA2 (ORF and 3'-UTR)-term <sub>ADH1</sub>
pVD787	pVD570 hsc82Δ::URA3
pVD788	pVD570 sis1Δ::URA3

pVD789	pVD570 <i>ydj1Δ::URA3</i>
pVD790	pVD576 <i>aha1Δ::URA3</i>
pVD791	pVD576 <i>fes1Δ::URA3</i>
pVD792	pVD576 <i>ssa2Δ::URA3</i>
pVD793	pVD576 <i>sti1Δ::URA3</i>
pVD794	pNH605 Pr <sub>ACT1</sub> -Z <sub>4</sub> EV-term <sub>ADH1</sub> – 6xZ <sub>4</sub> BS-Pr <sub>CYC1</sub> -term <sub>ADH1</sub>
pVD795	pNH605 Pr <sub>ACT1</sub> -Z <sub>4</sub> EV-term <sub>ADH1</sub> – 6xZ <sub>4</sub> BS-Pr <sub>CYC1</sub> -HSC82 (ORF and 3'-UTR)-term <sub>ADH1</sub>
pVD796	pNH605 Pr <sub>ACT1</sub> -Z <sub>4</sub> EV-term <sub>ADH1</sub> – 6xZ <sub>4</sub> BS-Pr <sub>CYC1</sub> -SSA2 (ORF and 3'-UTR)-term <sub>ADH1</sub>
pVD797	pNH605 6xZ <sub>4</sub> BS-Pr <sub>CYC1</sub> -HSC82 (ORF and 3'-UTR) – Pr <sub>ACT1</sub> -Z <sub>4</sub> EV-term <sub>ADH1</sub> – 6xZ <sub>4</sub> BS-Pr <sub>CYC1</sub> -SSA2 (ORF and 3'-UTR)-term <sub>ADH1</sub>
pVD902	pRS306 Pr <sub>ADH1</sub> -Gal4 DBD-ER-Msn2 AD-term <sub>ADH1</sub> – Pr <sub>Hsf1&amp;Gal4</sub> -GFP-term <sub>ACT1</sub> – Pr <sub>Gal4</sub> -mKATE2-term <sub>ADH1</sub>

**Stable genome modifications.** All strains are in the W303 genetic background. PCR-mediated gene deletion and gene tagging was carried out as described (Longtine et al., 1998). Cassettes for β-estradiol-dependent expression of *HSC82* and *SSA2* were targeted to the *HIS3* locus by homologous recombination as described (Sikorski and Hieter, 1989).

**FRB tagging.** Constructs for FRB and FRB-GFP tagging with either the *HIS3* or *KANMX* marker genes were obtained from EUROSCARF and described elsewhere (Haruki et al., 2008).

**Hsf1 reporter.** *Pr<sub>TEF2</sub>-mKATE-URA3-4xHSE-Pr<sub>CYC1</sub>-GFP* was PCR amplified from genomic DNA obtained from previously described strains containing the Hsf1 reporter (Brandman et al., 2012) and integrated into the *ura3-1* locus. *URA3* was eliminated from the reporter cassette in VDY2595 by transforming cells with a PCR amplicon of the *ura3-1* locus of wild-type W303 and counterselecting for *ura3*<sup>-</sup> transformants on 5-FOA.

**pHsf1 construction.** PCR amplicon comprising the Hsf1 promoter, open reading frame and 3' UTR obtained from wild-type yeast genomic DNA (Novagen) was ligated into BamHI-linearized pRS413 (Sikorski and Hieter, 1989) using Gibson assembly (Gibson

et al., 2009) to generate pVD476. A second construct with an alternate marker gene was generated by subcloning the NotI/XbaI fragment of pVD476 into the corresponding sites on pRS412 (Brachmann et al., 1998) to generate pVD565.

mCherry-Ubc9 constructs. pESC vectors for expressing mCherry-Ubc9 wild type (pVD380) and -ubc9<sup>ts</sup> (Ubc9 Y68L) (pVD381 and pVD632) were obtained from Stratagene and described elsewhere (Kaganovich et al., 2008).

pRS412 ade2Δ::HPHMX. To create the HPHMX-marked pRS41x-series plasmid pVD579, the backbone of pRS412 was digested to remove the BstAPI fragment (*ADE2* promoter and first 721bp of the ORF) and ligated to an HPHMX cassette amplicon from pAG32 (Goldstein and McCusker, 1999) by Gibson assembly (Gibson et al., 2009).

Construction of synHDG expression plasmids (pA-D). To engineer high levels of constitutive expression of Hsf1-dependent genes (HDGs) without Hsf1, we PCR amplified *ADH1*, *CYC1*, *PKG1*, *TDH3*, and *TEF1* promoters and HDG ORFs (with endogenous 3' UTRs) from genomic DNA (Novagen). Promoter sequences were first fused to the start codon of the HDG ORF by overlap-extension PCR (OE-PCR). Gibson assembly (Gibson et al., 2009) was then used to ligate promoter-ORF-UTR fusions into linearized *CEN/ARS* plasmids. The resulting plasmids were validated by sequencing. pA and pB vectors carrying single synHDG gene deletions were made by PCR-mediated gene deletion in yeast followed by plasmid recovery using a miniprep column (Qiagen) and sequence validation. Primer sequences used to construct pA-D are available upon request.

Construction of synHsp70/90 cassettes. To engineer β-estradiol-dependent expression of *HSC82* and *SSA2*, we PCR amplified ZEV promoter (consisting of 6×Z4 zinc-finger array binding sites (McIsaac et al., 2013)—Z<sub>4</sub>BS—upstream of a minimal *CYC1*-promoter), *HSC82* and *SSA2* ORFs (with endogenous 3' UTRs), and an expression cassette for ZEV (a chimeric transcription factor comprising Z4 zinc finger array -

estrogen receptor - VP16 activation domain that is activated by the hormone β-estradiol (McIsaac et al., 2013)). ZEV promoter was fused to the start codon of the *HSC82* and *SSA2* ORFs by OE-PCR. Gibson assembly was then used to ligate ZEV promoter-ORF fusions (or a control empty ZEV promoter with no downstream ORF) and ZEV expression cassette into linearized pRS416 to generate pVD783-786. NotI/Xhol fragments from the resulting plasmids containing the control promoter, synHsp70, synHsp90, or both were subcloned into pNH605 to generate pVD794-797. SfII digestion of the resulting plasmids produced *Pr<sub>ScLEU2</sub>-CgLEU2-ZEV-6xZ<sub>4</sub>BS-Pr<sub>CYC1</sub>-ORF(s)-3'-UTR<sub>ScLEU2</sub>* linear fragments that were each integrated separately at the *leu2* genomic locus by yeast transformation.

#### **Yeast media and growth conditions.**

Cells were grown at 30°C with shaking unless noted otherwise. Plasmid selection was maintained at all times by growing cells in standard synthetic media lacking the appropriate amino acid(s)/nucleotide base(s). All synthetic media contained dextrose (2%) as the carbon source, except for those used to induce expression of Ubc9<sup>wt</sup> and ubc9<sup>ts</sup>, which contained 2% raffinose + 2% galactose. All synthetic media were supplemented with 100mg/L adenine to suppress the growth defect and autofluorescence caused by the *ade2-1* mutation in the W303 genetic background, except for those used to select for *ADE2*-marked plasmids. All synthetic media contained ammonium sulfate as the nitrogen base, except for those used to select for *HPHMX*-marked plasmids, which contained 1g/L monosodium glutamate to enable selection with 200 mg/L Hygromycin B (Invitrogen).

#### **Mammalian cell lines, tissue culture, genetic manipulation and validation.**

Wild-type murine embryonic fibroblasts (MEFs) and embryonic stem cells (mESCs) were obtained from Jackson Laboratories (Immortalized MEFs: CBA316; mESCs: 129X1/SvJ strain).

#### Growth of mouse embryonic fibroblasts.

MEFs were cultured at 37°C in DMEM with 10% FBS, antibiotics 100 µM nonessential amino acids (Invitrogen, 11140-050), 2 mM L-glutamine (Invitrogen, 25030-081) and 100 U/ml penicillin/100 µg/ml streptomycin (Invitrogen, 15140-122).

Growth and maintenance of pluripotent mouse embryonic stem cells.

mESCs were cultured on a feeder layer of mitomycin C-treated MEFs with 0.2% gelatinized (Sigma, G1890) tissue culture plates in ESC media containing DMEM-KO (Invitrogen, 10829-018) supplemented with 15% fetal bovine serum, 1000 U/ml LIF (ESGRO, ESG1106), 100 µM nonessential amino acids (Invitrogen, 11140-050), 2 mM L-glutamine (Invitrogen, 25030-081), 100 U/ml penicillin, 100 µg/ml streptomycin (Invitrogen, 15140-122), and 8 nL/ml of 2-mercaptoethanol (Sigma, M7522).

Generation of *hsf1*<sup>-/-</sup> cell lines using CRISPR/Cas9. A single guide RNA (sgRNAs) targeting exon 1 of murine *HSF1* was designed using the Broad Institute Web interface (Doench et al., 2014). A single plasmid based on the pcDNA3-hCas9 plasmid (Mali et al., 2013) that includes both Cas9 expressed from the CMV promoter and the sgRNA expressed from the U6 promoter was transiently transfected into immortalized MEFs and mESC. Following NEO selection for plasmid uptake, single cells were obtained by limiting dilution and allowed to grow into colonies. Colonies were picked by microdissection and allowed to proliferate in 6 well plates. Isolated lines were screened by PCR and sequencing for the presence of a lesion in exon 1.

Western blotting:

To determine the effect of Hsf1 anchor away on Ssa1 and Hsc82 expression, cells were grown to mid-log in YPD at 30°C, backdiluted to OD<sub>600</sub> 0.2, split into two, and each half treated with 1µM rapamycin for the indicated times. 0.05 OD<sub>600</sub> was removed at each timepoint and treated with 10% TCA on ice for 1 hour before pelleting the cells and washing them with acetone. Washed pellets were air dried and then lysed by bead-beating in 50 mM Tris-HCl pH 7.5, 1mM EDTA, 1% SDS, and 2M urea. After measuring lysate protein concentrations using BCA (Pierce), equal amounts of protein were

resolved by SDS-PAGE (Invitrogen 4-20% tris/glycine/SDS gel (for 1 h at 200V), and electroblotted onto Nitrocellulose membrane (Bio-RAD). Blots were blocked with 5% milk in TBST and left probing overnight with anti-Ssa1 (generous gift of E. Craig), Hsc82 (Abcam), and Hxk1 (United States Biological) primary antibodies. Blots were washed 3x with TBST and probed with anti-rabbit Cy5-conjugated secondary antibody (Invitrogen). Blots were scanned on the Typhoon imaging system.

To validate *HSF1* gene knockout in mammalian cells, whole cell lysates were prepared using the mammalian protein extraction reagent (M-PER, Life technologies) according to manufacturer's instructions. Lysate proteins were resolved by SDS-PAGE (4-15% gradient tris/glycine/SDS gel (for 1 hour at 30 mA) and electroblotted onto PVDF membrane (Millipore) for 1 hour at 225 mA. Blots were blocked with Li-Cor blocking buffer (Li-Cor) and probed with anti-HSF1 (Cell Signaling #4356) and anti-ACT (Sigma A2066) primary antibodies. Blots were washed 3x with TBST and probed with anti-rabbit-800 IR conjugated secondary antibody (Li-Cor). Blots were scanned on the Li-Cor IR imaging system.

#### Immuno-flourescence.

Cells were seeded on 8-well chamber slides (Lab-Tek) for 18 hr prior to processing for immunofluorescence. Following cell fixation with 4% paraformaldehyde in PBS pH 7.4 for 10 minutes, slides were rinsed with phosphate-buffered saline (PBS) and blocked for 1 hr at room temperature with 0.5% bovine serum albumin (BSA) in PBS. After overnight incubation at 4°C with an anti-HSF1 rabbit antibody diluted 1:1000 (Cell Signaling #4356), slides were washed three times (5 min each time) with PBS and then incubated for 1 hr at room temperature in a secondary anti-rabbit antibody labeled with Alexa Dye 488 diluted 1:1000 (Molecular Probes). Lastly, slides were washed three additional times with PBS before mounting them with antifade reagent containing DAPI (Life Technologies P-36931) and imaged using a Zeiss epifluorescence microscope with a 40x objective.

### **Yeast cell fluorescence microscopy.**

ubc9<sup>ts</sup> aggregation assay. VDY2130 cells transformed with pVD380 or pVD381 were inoculated into SG/R-LEU media and grown overnight to OD<sub>600</sub> ≈ 0.1. Cells were then treated with 10 μM rapamycin for the indicated times and then fixed in ice-cold 4% formaldehyde in PBS pH 7.4 for 10 minutes. Fixed cells were imaged with an oil-immersion 63xobjective (63x, NA 1.4, oil Ph3, Plan - Apochromat) on an AxioObserver Z1 inverted microscope (Zeiss) equipped with a CoolSNAP-HQ CCD camera (Photometrics) and LED excitation (Colibri). Blinded images were background subtracted and at least 100 cells scored manually after local contrast optimization for mCherry foci using ImageJ. Note that local contrast optimization was necessary due to plasmid copy number variation, a known feature of 2<sup>+</sup> plasmids, which resulted in some cells with very high expression of mCherry-Ubc9 fusions that dominated global contrast optimization.

VDY2578 transformed with pVD632 and 15synHDGs (pVD576, pVD577, pVD578 and pVD580) or pHsf1 (pRS412, pRS415, pVD476 and pVD579) or empty vectors (pRS412, pRS413, pRS415 and pVD579) were assayed as above, except after growth in SG/R-ADE-HIS-LEU-URA containing 200 μg/ml hygromycin-B (Invitrogen).

VDY2130 transformed with pVD632 and cassettes from pVD794, 795, 796 or 797 were assayed as above, except after growth in SG/R-URA and pre-treatment with 10 μM β-estradiol.

Confocal live-cell microscopy. 96 well glass bottom plates were coated with 100 μg/ml concanavalin A in water for 1 hour, washed three times with water and dried at room temperature. 80 μl of low-density cells were added to a coated well. Cells were allowed to settle and attach for 15 minutes, and unattached cells were removed and replaced with 80 μl SD media. Imaging was performed at the W.M Keck Microscopy Facility at the Whitehead Institute using a Nikon Ti microscope equipped with a 100x, 1.49 NA

objective lens, an Andor Revolution spinning disc confocal setup and an Andor EMCCD camera.

To monitor the effect of rapamycin on Hsf1-FRB-GFP localization in VDY1877, cells were logarithmically grown in SD media to maintain OD<sub>600</sub> below 0.1 for 8 hours and attached to the glass bottom of a 96 well plate as described. Hsf1 nuclear depletion was performed with 1  $\mu$ M rapamycin added directly to the 80  $\mu$ l of media in the wells of the 96 well plate, and cells were imaged over time as described using the spinning disc microscope setup. Contrast was adjusted globally and images were cropped for presentation in Photoshop.

To monitor protein aggregation in live cells, identical strains were grown under the same conditions as the fixed protein aggregation assay and maintained at OD<sub>600</sub> less than 0.1 for 8 at least hours before starting the treatments. Cells were attached to the glass bottom of a 96 well plate as described. For heat shock experiments, cells were incubated in the plate at 37°C for 15 minutes before imaging. Hsf1 nuclear export was induced with 1  $\mu$ M rapamycin as described for the times indicated prior to imaging using the spinning disc microscope setup. Note that local contrast optimization was again necessary due to mCherry-Ubc9 plasmid copy number variation as described above. Contrast adjustment and cropping were performed in Photoshop.

Analysis of Hsf1 nuclear localization. DPY813 cells were grown for 18 hours in synthetic complete media with dextrose to OD<sub>600</sub> ~ 0.2 and diluted to OD<sub>600</sub> = 0.08 followed by treatment with 1  $\mu$ M rapamycin or mock treatment. 80  $\mu$ l of each sample was transferred to ConA-coated wells in a 96 well plate and incubated at 30°C for 15 minutes before imaging with spinning disc confocal microscopy. Contrast was adjusted globally and images were overlayed in Photoshop and presented as whole 512x512 pixel images or cropped, as indicated. Quantification of nuclear GFP fluorescence was performed in ImageJ. Masks defined by the NLS-mKate2 images were applied to the Hsf1-FRB-GFP channel and non-nuclear signal was removed. Maximum GFP intensity

was measured for each nucleus and for the background of each original GFP image. Background intensity was subtracted from each cell's nuclear GFP signal and the mean and standard error of the background-subtracted nuclear GFP signal were calculated and plotted for untreated and rapamycin-treated cells. Line-scan profiles across the nucleus for representative cells were also background-subtracted and plotted.

### **Analysis of transcriptional reporters by flow cytometry.**

Hsf1 DNA binding transcription factor competition assay. VDY1874 and VDY1896 cells with expressing GEM + prHsf1&Gal4-GFP + prGal4-mKATE2 from a pRS306 vector integrated at the *URA3* locus were inoculated into SD-URA media and grown overnight to  $OD_{600} \approx 0.1$ . Following transfer to a 96-well plate, cells were treated with 10  $\mu M$  rapamycin or carrier-only (90% EtOH, 10% Tween-20) and  $\beta$ -estradiol or carrier only (100% EtOH) for 90 minutes at 30°C. Single-cell GFP and mKate2 fluorescence was measured for ~10,000 cells using a LSRII (BD) flow cytometer. Single cell single-color fluorescence values were normalized by dividing by side scatter from the same cell, and GFP/RFP ratios were determined by dividing GFP by mKate fluorescence from the same cell. These values were then rescaled by dividing by the median value for double-mock treated cells. Custom R scripts that were used to analyze the fluorescence data are available upon request.

Hsf1-AA heat shock experiments. VDY1852 cells transformed with pRS412 or pVD565 were inoculated into SD-ADE media and grown overnight to  $OD_{600} \approx 0.1$ . Following transfer to a 96-well plate and pretreatment with 10  $\mu M$  rapamycin or carrier-only (90% EtOH, 10% Tween-20) at 30°C for 10 minutes, cells were split into two plates: one that was heat-shocked at 39°C for 30 minutes using a C1000 Touch thermal cycler (Bio Rad), the other control plate was immediately analyzed. Single-cell GFP and mKate fluorescence was measured for ~10,000 cells using a LSRII (BD) flow cytometer. Single cell fluorescence values were normalized by dividing GFP by mKate fluorescence from the same cell, and then these values were rescaled by dividing by the median

GFP/mKate value for VDY1852 + pRS412 cells after mock pretreatment without heat shock. Custom R scripts that were used to analyze the fluorescence data are available upon request.

Effect of synHDG expression on Hsf1 reporter. VDY2367 transformed with 15synHDGs (pVD576, pVD577, pVD578 and pVD580) or empty vectors (pRS412, pRS413, pRS415 and pVD579) were grown in SD-ADE-HIS-LEU media containing 200 µg/ml hygromycin-B (Invitrogen) overnight at 30°C to a final density of OD<sub>600</sub> ≈ 0.1 before being analyzed as the control plate above.

**Colony growth assays.** Cells transformed with synHDG plasmids and matching control vectors were inoculated into SD plasmid selection media with 10µM β-estradiol, if appropriate. After overnight growth to OD<sub>600</sub> ≈ 0.2, equal numbers of cells were harvested and serially diluted into fresh media in 96-well plates before being spotted with a multi-channel pipette or a 36-well pinning tool onto corresponding SD selection plates with 10µM rapamycin or carrier control (90% EtOH, 10% Tween-20). Plates were parafilmed and incubated at 30°C for 3-5 days before imaging with an Alpha Imager (Alpha Innotech).

#### **Native elongating transcript sequencing (NET-seq).**

For the NET-seq analysis of basal transcription, VDY2254 cells were grown overnight in 5 × 1L YPD (1% yeast extract, 2% peptone, 2% dextrose) at 30°C with shaking until they reached OD<sub>600</sub> ≈ 0.3. One culture was harvested by filtration onto a 90-mm diameter 0.45µm filter (Whatman) and cells scraped with a cooled spatula and transferred to liquid N<sub>2</sub>. Other cultures were treated with rapamycin (1µM) for 15, 30 and 60 minutes prior to harvesting as described above. For the NET-seq analysis of heat shock transcription, VDY2254 cells were grown overnight in 2L YPD to mid-log at 30°C until they reached OD<sub>600</sub> ≈ 0.66. The culture was then split equally and one half treated with rapamycin (1µM) and the other half left untreated. After further incubation with

shaking for 10 minutes at 30°C, each half was mixed with 1L of 50°C YPD and moved to to 39°C shaking water bath for 30 minutes prior to harvesting as described above.

Each sample was lysed frozen in a ball mill (Retsch). Rpb3 immunoprecipitation from lysates and sequencing library creation from immunopurified RNA was carried out as described (Churchman and Weissman, 2011) with one notable difference: circularized cDNA samples were barcoded during PCR amplification to enable multiplexing in an Illumina Hi-Seq 2500 (Bauer Core Facility). Reads were assigned by the barcode to the appropriate sample. Sequenced nascent transcript fragments were groomed and aligned to the *S. cerevisiae* ORF coding reference genome using Bowtie before being assembled and quantified using Cufflinks. Fold changes were computed using Cuffdiff.

### **Yeast RNA-seq.**

Cells were grown in YPD overnight at 30°C with shaking until they reached OD<sub>600</sub> ≈ 0.5. Cultures were split into 5 ml aliquots before indicated treatments. 1.5 ml of treated cells were harvested by spinning for 30 seconds at 15,000 rpm speed in an Eppendorf 5430 benchtop centrifuge and snap frozen before storage at -80°C. The small culture volume and quick spin obviated the need for filtration. Frozen cell pellets were thawed on ice, resuspended in 1 ml water, transferred to fresh 1.5 ml tubes and harvested by spinning as above. Washed cell pellets were resuspended in 200 µl AE (50 mM NaOAc, pH 5.2, 10 mM EDTA) and vortexed. 20 µl of 10% SDS was added, followed by 250 µl acid phenol, and samples were incubated at 65°C with shaking for 10 minutes. After an additional 5 minutes on ice, samples were spun at 15,000 rpm for 5 minutes at 4°C. Supernatants were transferred to pre-spun heavy phase lock tubes (5 Prime) and 250 µl chloroform was added. Tubes were spun at full speed for 5 minutes at 15,000 rpm and aqueous layers (above the wax) were transferred to fresh 1.5 ml tubes. 30 µl of 3M NaOAc, pH 5.2 was added followed by 750 µl ice cold 100% ethanol. RNA was precipitated at -80°C for 30 minutes and samples were spun at 15,000 rpm for 30 minutes at 4°C. Pellets were washed with 1 ml 70% ethanol, spun at 15,000 rpm for 10 minutes at 4°C for. The supernatant was removed and pellets were allowed to dry on ice

for 10 minutes. Lastly, RNA pellets were resuspended in 30  $\mu$ l DEPC water and the RNA concentrations of the resulting solutions measured by Nano Drop.

Total RNA samples were submitted to the Whitehead Institute Genome Technology Core (WIGTC) where polyA + RNA was purified, fragmented and sequencing libraries barcoded to enable multiplexing in an Illumina Hi-Seq 2500. Reads were assigned by the barcode to the appropriate sample.

Data were processed using a local version of the Galaxy suite of next-generation sequencing tools. Sequenced mRNA fragments were groomed and aligned to the *S. cerevisiae* ORF coding reference genome (Feb. 2011) using Tophat before being assembled and quantified using Cufflinks. Fold changes were computed using Cuffdiff.

### **Defining Hsf1-dependent genes in yeast.**

Significance analysis of transcription under basal conditions. Hsf1-dependent genes were defined by combining statistical analyses of NET-seq and RNA-seq data. First, we used the CuffDiff (Trapnell et al., 2012) time series analysis algorithm to jointly analyze the NET-seq time course (15, 30, and 60 minutes of rapamycin treatment). We identified genes with significantly different transcription after 15 minutes that persisted for the remainder of the time course (no additional significant changes at the 30 or 60 minute time points). This analysis identified 30 genes that met these criteria using the most stringent p-value cutoff of  $p < 10^{-4}$ . We then tested whether these genes had significant changes in mRNA levels measured by RNA-seq that were caused by 60' of rapamycin treatment. We used genes without significant NET-seq changes to construct a null distribution of fold-changes. Using the 1<sup>st</sup> and 99<sup>th</sup> percentile of the null fold-change distribution as cutoffs, we identified 18 of the initial 30 gene as also having significant differences in mRNA levels.

Analysis of SSA1 and SSA2 sequencing data. The 94% sequence identity between the open reading frames for SSA1 and SSA2 makes computational deconvolution of

sequencing reads between the two paralogs unreliable. Thus, we averaged the FPKM values for the two genes into one *SSA1/2* value for the NET-seq and ChIP-seq analysis in Figure 2a,b. As the two genes are computational indistinguishable by mRNA-seq, we focus the remainder of our expression analysis on *SSA2*, which has ~5-fold greater expression than *SSA1*, with the caveat that a fraction of *SSA2* reads are likely from *SSA1*.

Statistical analysis of Hsf1-dependent gene expression during heat shock. In contrast to the small number of gene expression changes induced by short-term rapamycin treatment of Hsf1-AA cells at 30°C, rapamycin pre-treatment induced correlated changes in transcription and mRNA abundance of hundreds of genes during subsequent heat shock. As the cuff-diff algorithms for computing p-values and false discovery rates become less reliable when there are large-scale expression changes (Trapnell et al., 2012), we decided to use a non-parametric, rank-based statistical significance analysis for changes to both transcription and mRNA abundance. We defined Hsf1-dependent gene expression during heat shock as those genes that fell below the 10<sup>th</sup> percentile for both the NET-seq and RNA-seq datasets comparing rapamycin pre-treated versus mock pre-treated heat shock samples. As these two datasets were collected during independent experiments, we were comfortable assuming that the random factors that drive false discovery are independent and therefore the false discovery rate should be limited to 1% overall. We considered alternative significance thresholds for our rank-based analysis, but bioinformatic analysis of significant genes suggested that the 10% threshold optimized our sensitivity to detect small, coherent changes without a high rate of false discovery, as judged by the relative enrichment for GO terms and promoter motifs between the different significance thresholds.

Bioinformatic analysis of gene expression changes during heat shock absent Hsf1 function. To measure Hsf1-dependent gene expression during heat shock, we used NET-seq and RNA-seq to monitor the effect of a brief rapamycin pre-treatment on the

heat shock response of Hsf1-AA cells. This analysis revealed a much larger number of changes than we had observed by rapamycin treatment of cells in the absence of stress, which necessitated changes to our statistical analysis (see above). We defined a set of 295 genes that had significantly reduced transcription and mRNA abundance in comparison to heat shock of mock pre-treated cells (Figure S3H). Gene ontology analysis revealed enrichment for various protein synthesis and metabolic functions (Figure S3J) while promoter analysis revealed enrichment ( $p$ -value  $< 10^{-64}$ ) for binding sites of Sfp1, a canonical regulator of ribosome biogenesis (Fingerman et al., 2003; Jorgensen et al., 2004; Marion et al., 2004). In fact, 103/295 affected genes were ribosomal protein genes (RPGs) (enrichment  $p$ -value  $< 10^{-116}$ ) (Nakao et al., 2004), which heat shock normally represses and which were repressed even further as a gene set by rapamycin pre-treatment ( $p < 10^{-64}$ ) (Figure S3I). An additional 144 affected genes had predicted Sfp1 binding sites in their promoters (Figure S3H,J) suggesting co-regulation with RPGs through heat inactivation of the transcriptional activator Sfp1 (Marion et al., 2004). One potential explanation for the genome-wide over-repression of Sfp1 gene targets is that rapamycin pre-treatment potentiates the strength of heat as a stimulus, similar to the way in which partial loss-of-function mutations in Hsf1 sensitize cells to heat stress (Imazu and Sakurai, 2005; Morano, 1999; Morano et al., 1999; Smith and Yaffe, 1991). As an independent test of this idea, we re-visited heat shock induced gene induction by Msn2/4 and found a significant over-induction of Msn2/4 gene targets relative to all other genes ( $p$ -value  $< 10^{-46}$ ) (Figure S3I). We conclude by speculating that even a short rapamycin pre-treatment of Hsf1-AA cells reduces chaperone expression enough to potentiate regulation of Sfp1 and Msn2/4 gene targets by heat-induced proteotoxicity.

Having found no compelling evidence that Hsf1 directly regulates 247/295 genes defined by our gene expression analysis we looked more closely at the remaining 48. Among these, we found a subset of basal HDGs (6/18), all but one of which lacked Msn2/4 binding sites in their promoters. We note that the 18 basal HDGs, as an entire set, had a significant ~5-fold decrease in median mRNA abundance ( $p$ -value  $< 10^{-5}$ )

relative to all other genes (Figure S3I). Along the same lines, heat shock induction of *SSA3* and *SSA4*, which encode Hsp70 paralogs that lack significant basal expression at 30°C, was strongly reduced by rapamycin pre-treatment (Figure S3H). Lastly, we found no common themes by either promoter motif or gene ontology analysis among the remaining 40 affected genes (Figure S3J). We note that the size of this seemingly random gene set is consistent with the false discovery rate (FDR) for our statistical analysis (at our theoretical 1% FDR, we would expect ~46 false discoveries by chance from the total population of 4590 detected genes).

To independently test if Hsf1-dependent genes defined by the NET-seq/RNA-seq analysis of heat shock are *bona fide* Hsf1 gene targets, we measured Hsf1 DNA binding during heat shock by chromatin immunoprecipitation followed by deep sequencing (ChIP-seq). As before, we isolated chromatin using tandem affinity purification of dual epitope-tagged Hsf1-FLAG-V5 expressed as the only copy of Hsf1 in an otherwise wild type genetic background. Analysis using a stringent peak-calling algorithm (see below) defined 32 Hsf1 gene targets, including all 18 HDGs ( $p\text{-value} < 10^{-36}$ ) and, more broadly, 27/40 genes we previously defined by ChIP-seq analysis of basal targets ( $p\text{-value} < 10^{-59}$ ) (Figure S3G). By contrast, only 8 of these gene targets were among the 296 genes defined by our heat shock gene expression analysis: 5 of the original 18 basal HDGs, *SSA4*, *SSE1* (a member of the Hsp110 branch of the Hsp70 family), and *HSP10* (a mitochondrial matrix co-chaperonin). We note that for certain non-HDGs in this overlapping set (e.g., *SSE1*) under basal conditions we detected significant Hsf1 promoter binding and Hsf1 AA was associated with small—but not statistically significant—decreases in their expression (Figure S2I), thus raising the possibility that they make a small but real fitness contribution as HDGs even in the absence of stress.

In summary, our combined NET-seq/RNA-seq/ChIP-seq analysis provides little evidence for significant expansion of Hsf1's gene targets beyond HDGs during heat shock. Rather, it argues that Hsf1's primary role during heat shock is to overexpress key chaperones that are already under its basal control.

### **Defining Msn2/4 target genes.**

Msn2/4 targets were defined as those genes in the top 10% of expression changes induced by 1-NM-PP1 treatment of PKAas cells that also contained at least one Msn2/4 binding site (AGGGG) in their promoter (defined as the intergenic region between the start codon of the gene of interest and the start or stop codon of the closest 5' open reading frame) using SCOPE (Carlson et al., 2007).

### **Defining ribosomal protein genes and Sfp1 targets.**

Yeast genes that encode ribosomal proteins are easily identified based on their RPL-, RPS- and RPP- gene name prefixes to denote components of the large and small ribosomal subunits, along with other ribosomal proteins (Nakao et al., 2004). Their expression is transcriptionally controlled by Sfp1, which has a known promoter binding site (AAA[A/T]TTTT) (Fingerman et al., 2003; Jorgensen et al., 2004). Among the 295 genes with significant changes in heat shock expression due to Hsf1 AA, we found 103 RPL/RPS/RPP genes, plus 144 additional genes that had at least one Sfp1 binding site in their promoter (defined as the intergenic region between the start codon of the gene of interest and the start or stop codon of the closest 5' open reading frame) using SCOPE (Carlson et al., 2007).

### **Mammalian cell RNA-seq.**

MEFs and mESCs were cultured to 75% confluence in 10 cm dishes as described above. Heat shock was performed by transferring dishes to a 42°C incubator for 1 hour. Total RNA was extracted using RNeasy kits (Qiagen) according to the manufacturer's directions. Sequencing libraries were prepared and sequenced by the WIGTC as described above. Data was processed using Galaxy, aligned to the annotated Mm10 genome and quantified as described above.

### **Defining HSF1-dependent changes in gene expression during heat shock in mammalian cells.**

In general, we found that changes in mammalian gene expression were smaller in both magnitude and the number of genes affected compared to yeast. While in each gene expression analysis most genes were highly correlated, the variance was not constant across genes—high expression genes tended to be less variable than low expression genes. To identify significant changes in gene expression, we needed a statistical inference strategy that accounts for the variance-expression relationship and adjusts the significance threshold accordingly. While there are parametric statistical inference methods that can account for non-constant variance, they require specification of a variance model and are very sensitive to its misspecification. Therefore, we choose to use a simple non-parametric approach based on quantile regression of gene expression levels between two samples to define significant changes. Intuitively, our strategy is similar to calling the top 1% of fold changes as significant, but the quantile regression allows us to take into account that the top 1% of fold changes for high expression genes will be smaller than for low expression genes. For example, by regressing the 99<sup>th</sup> percentile of heat shock gene expression on control expression, we obtain a linear function that defines for each control expression level a corresponding value that 99% of heat shock expression measurements should fall below. A similar regression for the 1<sup>st</sup> percentile of fold changes allowed us to define a lower significance threshold. Together these two regressions define an interval with 98% coverage both globally and locally. That is, using regression of heat shock expression on control as an example, heat shock expression for 98% of all genes will fall between their respective fitted values from the 1<sup>st</sup> and 99<sup>th</sup> percentile regressions, and further for any subset of genes with similar control expression approximately 98% of their heat shock expression values will fall between the regression fits. We defined genes above and below the bounds defined by these two regressions as significantly induced and repressed, respectively.

One caveat of this approach is that the number of changes that we call as significant for any experiment is set by design at 1% of the total number of genes. Even during heat shock, our exploratory analysis suggested that expression of less than 1% of genes was affected and therefore many significant changes defined by our analysis of a single

experiment will be false positives due to random variation. However, because we were ultimately interested in genes that have significant changes in *both* cell types, our false discovery rate due to random variation—which should be independent between cell types—is limited to .01%. Thus, the fact that we defined 129 heat shock induced genes in mESCs is not interpretable (since 129 is ~1% of the 13,356 genes detected), however that we defined 20 heat shock induced genes in both mESCs and MEFs is highly significant ( $p\text{-value} < 10^{-17}$ ), since the number of false discoveries should follow a binomial( $n= 13,356$ ,  $p= .0001$ ) distribution and therefore we expect to call only 1.3 significant genes in both cell types by random chance. One additional caveat of our analysis is that because the 1<sup>st</sup> and 99<sup>th</sup> percentile regressions are not parallel, they will cross and beyond this intersection the fit for the 1<sup>st</sup> percentile will be greater than that of the 99<sup>th</sup>. After this point, our interpretation of these as upper and lower bounds no longer holds and therefore their utility for our statistical inference breaks down. Our conservative approach to avoid this was to compare the quantile regression fits for the 1<sup>st</sup> and 99<sup>th</sup> percentiles to the median regression (50<sup>th</sup> percentile) fit, and exclude from our inference genes where the fit from the 1<sup>st</sup> percentile regression is greater than, or the 99<sup>th</sup> percentile fit is less than, the median regression fit. This approach, though conservative, affected a very small fraction of genes (~0.1%). For example, we excluded only 8/13,356 genes from our inference for heat shock analysis of mESCs.

We defined genes as HSF1-dependent if their expression was significantly induced by heat shock vs. control in wild type cells, and significantly reduced during heat shock in *hsf1*<sup>-/-</sup> vs. wild type cells, for both mESCs and MEFs. This analysis defined 9 HSF1-dependent genes. Since our statistical inference used expression from heat shocked wild type cells in both statistical tests for each cell type, we cannot comfortably assume that our inference was based on 4 independent tests—which would imply an over all false discovery rate of .01<sup>4</sup>, or  $10^{-8}$ ). However, even under the very conservative assumption that our inference is equivalent to just two independent statistical tests (one for each cell type), the probability of observing 9 (or more) significant genes is  $\sim 10^{-5}$ . We note that our choice of a 1% rate of false discovery for individual tests was based on

bioinformatic analysis of gene sets defined using alternative significance thresholds, which showed that the 1% level optimized sensitivity and specificity.

### **ChIP-PCR.**

Chromatin was prepared as described for ChIP-seq from the untagged AA parent (VDY1667) and the Hsf1-FRB AA strain (VDY1852) in the presence or absence of 1  $\mu$ M rapamycin for 15 minutes. Immunoprecipitation was performed with rabbit polyclonal anti-FRB antibody (Enzo Life Sciences) used at 1:200 and incubated on a rotator for 2 hours at 4°C followed by capture with 25  $\mu$ l 50% slurry of protein A/G Dynabeads (Thermo Fisher) for 1 hour at 4°C prior to magnetic separation. Washes and elutions were performed as described for the V5 step of the ChIP-seq protocol. PCR was performed using primers designed for 200 bp amplicons that spanned -100 to -300 bps with respect to the ATG start codon of the ORFs of *PHO5* (non Hsf1 target), *HSP82* and *SSA1* (Hsf1 targets). 2  $\mu$ l of the pooled whole cell extract (WCE) and each of the IP samples were used as templates in 25  $\mu$ l PCR reactions run for 30 cycles and the full reactions were run on a 1% agarose gel containing SybrSafe DNA gel stain (Thermo Fisher). Quantification was performed using ImageJ. To remove non-specific signal, we subtracted from the Hsf1-FRB values the band intensity of the identically-treated untagged-Hsf1 IP.

### **Chromatin immunoprecipitation and sequencing.**

50 ml of cells were grown to OD<sub>600</sub>=0.5. Cells were fixed with addition of 1% formaldehyde for 20 minutes at room temperature followed by quenching with 125 mM glycine for 10 minutes. Cells were pelleted, washed with ice-cold PBS. Pellets were frozen in liquid N<sub>2</sub> and stored at -80°C. Cells were lysed frozen in a coffee grinder with dry ice. After the dry ice was evaporated, lysate was resuspended in 2 ml ChIP buffer (50 mM Hepes pH 7.5, 140 mM NaCl, 1 mM EDTA, 1% triton x-100, 0.1% DOC) and sonicated 10 times using a probe sonicator (18W, 30 seconds on, one minute off) during which time they were kept on ice. 1 ml was transferred to a 1.5 ml tube and spun to remove cell debris. Input was set aside, and a serial IP was performed. First, 25  $\mu$ l of

anti-FLAG magnetic beads (50% slurry, Sigma) were added the mixture was incubated for 2 hours at 4°C on a rotator. Beads were separated with a magnet and the supernatant was removed. Beads were washed 5 times with 1 ml ChIP buffer (5 minute incubations at 4°C between each wash) and bound material eluted with 1 ml of 1 mg/ml 3xFLAG peptide (Sigma) in ChIP buffer by incubating at room temperature for 10 minutes. Beads were separated with a magnet and eluate was transferred to a fresh tube. Next, 25  $\mu$ l of anti-V5 magnetic beads (50% slurry, MBL International) were added and the mixture was incubated for 2 hours at 4°C on a rotator. Beads were separated with a magnet and the supernatant was removed. Beads were washed 3 times with 1 ChIP buffer, followed by a high salt wash (ChIP buffer + 500 mM NaCl) and a final wash in TE (all washes were with 1 ml with 5 minute incubations at 4°C between each wash). Bound material was eluted with 250  $\mu$ l TE + 1% SDS by incubating at 65°C for 15 minutes. Beads were separated with a magnet and eluate was transferred to a fresh tube and incubated overnight at 65°C to reverse crosslinks. Protein was degraded by adding 250  $\mu$ l 40  $\mu$ g/ml proteinase K in TE (supplemented with GlycoBlue to visualize subsequent pellets) and incubating at 37°C for 2 hours. DNA fragments were separated from protein by adding 500  $\mu$ l phenol/chloroform/isoamyl alcohol (25:24:1), and the aqueous layer was added to a fresh tube. 55  $\mu$ l of 4M LiCl was added along with 1 ml of 100% EtOH, and DNA was precipitated at -80°C overnight. DNA was pelleted by spinning at 15,000 rpm in an Eppendorf 5424 benchtop centrifuge for 30 minutes at 4°C and resuspended in 50  $\mu$ l TE. Sequencing libraries were prepared by the WIGTC, and sequenced on the Illumina Hi-Seq 2500. Reads were aligned to the yeast genome with Bowtie and Wiggle files were generated. Peaks were called with MACS v1.4.2 using a stringent p-value cutoff ( $p < 10^{-30}$ ).

### Promoter motif and gene ontology analysis.

Enrichment for DNA motifs was calculated using the SCOPE web interface (Carlson et al., 2007), and enrichment for gene ontology terms was calculated using YEAST Mine (Balakrishnan et al., 2012). Enrichment p-values for GO terms were corrected for multiple hypothesis testing using the Holm–Bonferroni correction implemented in

YEAST Mine. Gene set enrichment analysis for over-representation of one gene within another set was determined using the hypergeometric distribution.

### **Protein-protein interaction network analysis.**

Protein interaction networks were generated using the STRING database (Jensen, 2009). Yeast interactions were generated with a required confidence score of .90 and “Active Prediction Methods” based on experiments, co- occurrence and databases. Mouse interaction networks were generated with a required confidence score of 0.70 and “Active Prediction Methods” based on neighborhood, gene fusion, co-occurrence, experiments, databases and text mining. We explicitly did not allow co-expression data to be used in the network construction because HDGs were defined based on expression analysis and we wanted the protein-protein interaction network data to be derived from independent data sets. Also, we used a lower confidence threshold and additional data sources for construction of the mouse network because there was far less high-confidence experimental interaction data than for yeast resulting in an artificially sparse mouse network *ceteris paribus*.

### **SUPPLEMENTARY REFERENCES**

- Balakrishnan, R., Park, J., Karra, K., Hitz, B.C., Binkley, G., Hong, E.L., Sullivan, J., Micklem, G., Cherry, J.M., 2012. YeastMine--an integrated data warehouse for *Saccharomyces cerevisiae* data as a multipurpose tool-kit. Database (Oxford) 2012, bar062–bar062.
- Brachmann, C.B., Davies, A., Cost, G.J., Caputo, E., Li, J., Hieter, P., Boeke, J.D., 1998. Designer deletion strains derived from *Saccharomyces cerevisiae* S288C: a useful set of strains and plasmids for PCR-mediated gene disruption and other applications. Yeast 14, 115–132.
- Brandman, O., Stewart-Ornstein, J., Wong, D., Larson, A., Williams, C.C., Li, G.-W., Zhou, S., King, D., Shen, P.S., Weibezahn, J., Dunn, J.G., Rouskin, S., Inada, T., Frost, A., Weissman, J.S., 2012. A ribosome-bound quality control complex triggers degradation of nascent peptides and signals translation stress. Cell 151, 1042–1054.
- Carlson, J.M., Chakravarty, A., DeZiel, C.E., Gross, R.H., 2007. SCOPE: a web server for practical de novo motif discovery. Nucleic Acids Research 35, W259–64.
- Churchman, L.S., Weissman, J.S., 2011. Nascent transcript sequencing visualizes transcription at nucleotide resolution. Nature 469, 368–373.
- Doench, J.G., Hartenian, E., Graham, D.B., Tothova, Z., Hegde, M., Smith, I., Sullender,

- M., Ebert, B.L., Xavier, R.J., Root, D.E., 2014. Rational design of highly active sgRNAs for CRISPR-Cas9–mediated gene inactivation. *Nat Biotechnol* 32, 1262–1267.
- Fingerman, I., Nagaraj, V., Norris, D., Vershon, A.K., 2003. Sfp1 plays a key role in yeast ribosome biogenesis. *Eukaryotic Cell* 2, 1061–1068.
- Gibson, D.G., Young, L., Chuang, R.-Y., Venter, J.C., Hutchison, C.A., Smith, H.O., 2009. Enzymatic assembly of DNA molecules up to several hundred kilobases. *Nat Meth* 6, 343–345.
- Goldstein, A.L., McCusker, J.H., 1999. Three new dominant drug resistance cassettes for gene disruption in *Saccharomyces cerevisiae*. *Yeast* 15, 1541–1553.
- Haruki, H., Nishikawa, J., Laemmli, U.K., 2008. The Anchor-Away Technique: Rapid, Conditional Establishment of Yeast Mutant Phenotypes. *Mol Cell* 31, 925–932.
- Imazu, H., Sakurai, H., 2005. *Saccharomyces cerevisiae* heat shock transcription factor regulates cell wall remodeling in response to heat shock. *Eukaryotic Cell* 4, 1050–1056.
- Jensen, L.J., 2009. STRING 8---a global view on proteins and their functional interactions in 630 organisms. *Nucleic Acids Res* 37, D412–D416.
- Jorgensen, P., Rupes, I., Sharom, J.R., Schneper, L., Broach, J.R., Tyers, M., 2004. A dynamic transcriptional network communicates growth potential to ribosome synthesis and critical cell size. *Genes & development* 18, 2491–2505.
- Kaganovich, D., Kopito, R., Frydman, J., 2008. Misfolded proteins partition between two distinct quality control compartments. *Nature* 454, 1088–1095.
- Longtine, M.S., McKenzie, A., Demarini, D.J., Shah, N.G., Wach, A., Brachet, A., Philippse, P., Pringle, J.R., 1998. Additional modules for versatile and economical PCR-based gene deletion and modification in *Saccharomyces cerevisiae*. *Yeast* 14, 953–961.
- Mali, P., Yang, L., Esvelt, K.M., Aach, J., Guell, M., DiCarlo, J.E., Norville, J.E., Church, G.M., 2013. RNA-Guided Human Genome Engineering via Cas9. *Science* 339, 823–826.
- Marion, R.M., Regev, A., Segal, E., Barash, Y., Koller, D., Friedman, N., O'Shea, E.K., 2004. Sfp1 is a stress- and nutrient-sensitive regulator of ribosomal protein gene expression. *Proc Natl Acad Sci USA* 101, 14315–14322.
- McIsaac, R.S., Oakes, B.L., Wang, X., Dummit, K.A., Botstein, D., Noyes, M.B., 2013. Synthetic gene expression perturbation systems with rapid, tunable, single-gene specificity in yeast. *Nucleic Acids Research* 41, e57.
- McIsaac, R.S., Silverman, S.J., McClean, M.N., Gibney, P.A., Macinskas, J., Hickman, M.J., Pettit, A.A., Botstein, D., 2011. Fast-acting and nearly gratuitous induction of gene expression and protein depletion in *Saccharomyces cerevisiae*. *Mol Biol Cell* 22, 4447–4459.
- Morano, K.A., 1999. The Sch9 protein kinase regulates Hsp90 chaperone complex signal transduction activity in vivo. *EMBO J* 18, 5953–5962.
- Morano, K.A., Santoro, N., Koch, K.A., Thiele, D.J., 1999. A trans-activation domain in yeast heat shock transcription factor is essential for cell cycle progression during stress. *Mol Cell Biol* 19, 402–411.

- Nakao, A., Yoshihama, M., Kenmochi, N., 2004. RPG: the Ribosomal Protein Gene database. *Nucleic Acids Research* 32, D168–70.
- Sikorski, R.S., Hieter, P., 1989. A system of shuttle vectors and yeast host strains designed for efficient manipulation of DNA in *Saccharomyces cerevisiae*. *Genetics* 122, 19–27.
- Smith, B.J., Yaffe, M.P., 1991. A Mutation in the Yeast Heat-Shock Factor Gene Causes Temperature-Sensitive Defects in Both Mitochondrial Protein Import and the Cell-Cycle. *Mol Cell Biol* 11, 2647–2655.
- Trapnell, C., Roberts, A., Goff, L., Pertea, G., Kim, D., Kelley, D.R., Pimentel, H., Salzberg, S.L., Rinn, J.L., Pachter, L., 2012. Differential gene and transcript expression analysis of RNA-seq experiments with TopHat and Cufflinks. *Nat Protoc* 7, 562–578.